THE MAIN PHASE OF MAGNETIC STORMS AND THE RING CURRENT

SYUN-ICHI AKASOFU
Geophysical Institute, University of Alaska, College, Alaska, U.S.A.

(Received March 5, 1963)

1. Introduction

Magnetic storms are extremely complicated phenomena, but nevertheless two major average features can be found when magnetic records are collected from middle and low latitude observatories, well distributed around the earth. They are an initial positive phase in the horizontal force and a subsequent larger and more prolonged decrease, the main phase. Figure 1 illustrates the H variations during the July 11 and July 15, 1959 magnetic storms at ten low latitude observatories well distributed in longitude. Dotted curves are the H variations for the two intervals at the same hours of Greenwich time on July 13/14, during the quiet period between the two storms. These dotted curves may be taken to represent approximately the Sq variation (quiet-day solar daily magnetic variation). It is clear from the Figure that both the initial and the main phase occur on a worldwide scale. The nature of magnetic storms has been studied in great details by CHAPMAN and SUGIURA (1919, 1935); see also CHAPMAN and BARTELS (1940), CHAPMAN (1951), SUGIURA and CHAPMAN (1960). CHAPMAN expressed the average storm field D as the combination of an axially symmetric part Dst and the remainder SD. Because of the worldwide nature of the initial phase and the main phase, a substantial portion of them are expressed by the Dst component of D. The Dst variation can be defined for an average of a number of magnetic storms or for individual storms (see Appendix). Figure 2 shows the low latitude Dst curves for two of the July 1959 storms.

The Dst field is approximately uniform over the major part of the earth. Its field lines are parallel or anti-parallel to the dipole axis, and its primary cause is generally believed to be located far away from the earth, say a few earth radii, though there are some who dissent from this view. Because the earth is an electrically conducting sphere, any changes of external magnetic fields induce electric currents within the solid and liquid earth. It is found that the storm-time fields penetrate appreciably into the earth's crust and that the conductivity attained at depths of a few hundred km suffices to shield the deeper interior from the storm changes. The induced zonal currents produce an additional dipolar field outside the solid earth. Therefore, what we observe on the earth's surface is the combination of the external and induced Dst fields (see Appendix).

When magnetic storms occur successively, their Dst fields may be superposed on

Space Science Reviews 2 (1963) 91–135;

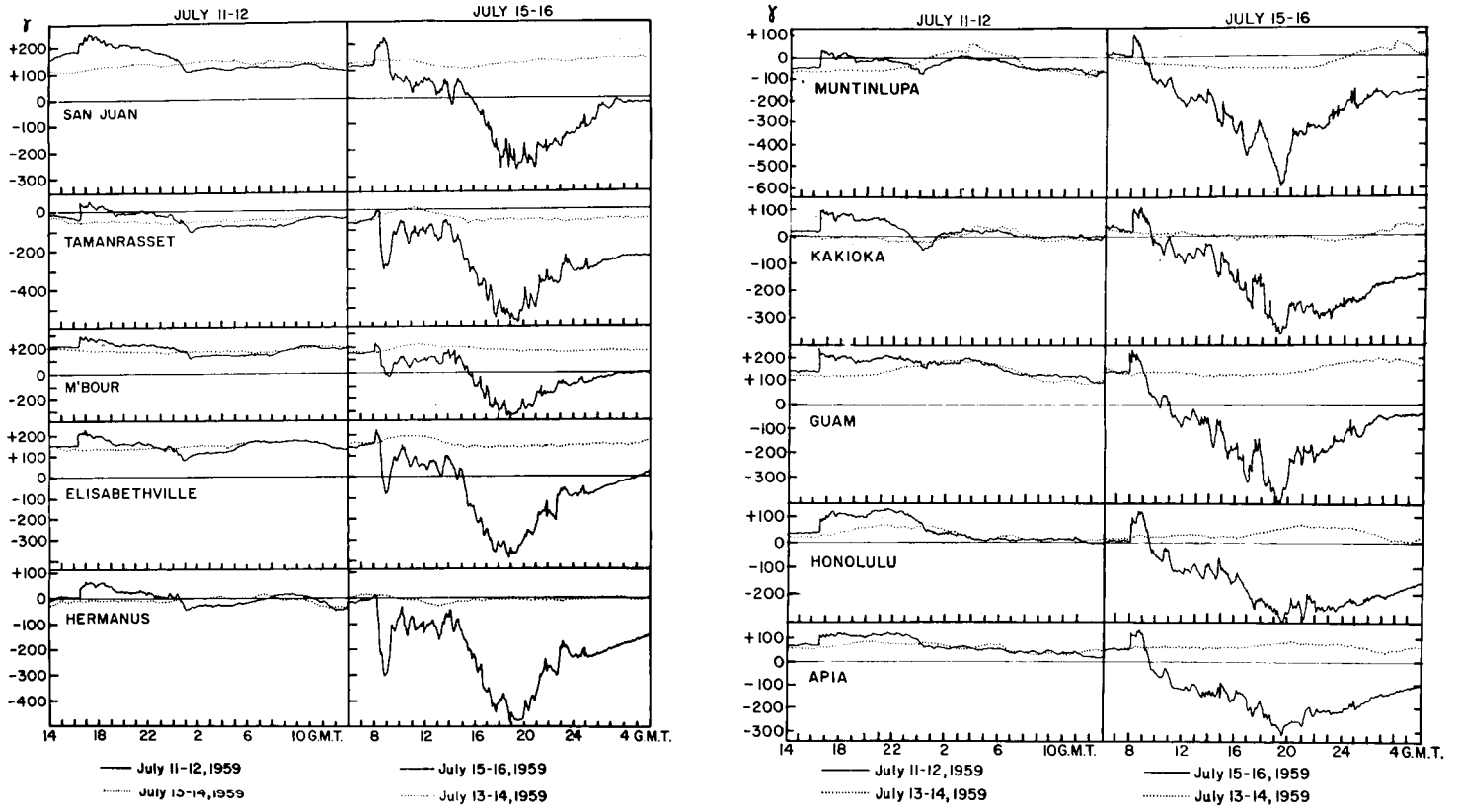

Fig. 1. The horizontal component magnetograms for 24 hour intervals beginning just before the storms of July 11/12, 1959 and July 15/16, 1959, from ten stations in relatively low latitudes. The dotted lines show the records from the same 24 hours of Greenwich time on July 13/14, 1959 (between the two storms), when the magnetic activity was low.

one another. Figure 3 shows such an example of the superposition of three successive Dst fields. After the maximum epoch of the main phase is reached, the main phase field diminishes, rapidly for the first 12 to about 24 hours and then more slowly.

Following CHAPMAN and FERRARO (1931), the initial positive phase is ascribed to the impact of solar plasma on the earth's magnetic field, and to the formation of a cavity around the earth in the plasma. The shape of the cavity has recently been extensively studied, using two or three dimensional models.

The main phase decrease has long been ascribed to a westward electric current encircling the earth. It is now generally called the "ring current". Although several attempts were made in the past to investigate the nature of the ring current (CHAPMAN and FERRARO, 1933; ALFVÉN, 1958), our present concept of the ring current is due to SINGER (1957), who initiated new studies based on ALFVÉN's guiding center approximation for the motion of charged particles in a dipole field, and to Van Allen and his associates, who discovered and explored the radiation belts.

In the following, we summarize present knowledge of the ring current, and discuss several important problems which must be explored further.

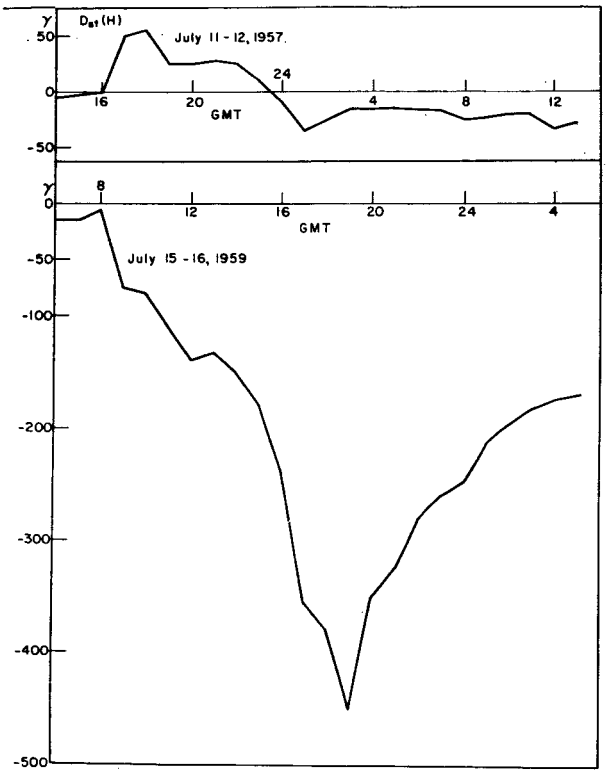

Fig. 2. The Dst(H') curves for the July 11, 1959 and July 15, 1959 storms from 12 low-latitude stations.

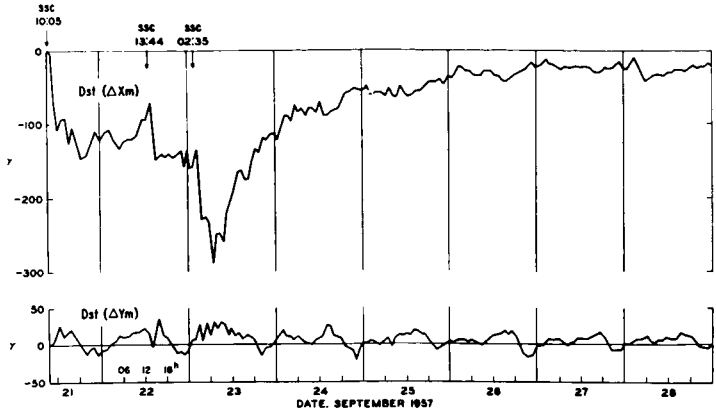

Fig. 3. The Dst(ΔX_m) and Dst(ΔY_m) curves for the September 21, 22 and 23 storms, obtained from 9 low-latitude stations. X_m and Y_m are the north-south and the east-west components, respectively in the geomagnetic coordinate system. (Dst(ΔX_m) $\simeq$ Dst(H')).

2. Motions of Charged Particles in a Dipole Field

The first extensive study of the trajectories of a charged particle in a dipole field was made by STÖRMER (1955), whose results are summarized in his *The Polar Aurora*. If STÖRMER's integration constant γ is larger than unity, there are two separate regions in which the trajectory can exist. One of the regions which extends to infinity is called the outer allowed region, and the other which is connected to the origin is called the inner allowed region (pp. 229–239).

Our particular concern here is the trajectories confined in the inner allowed region; one of such STÖRMER's trajectories is reproduced in a paper by VAN ALLEN (1961). Such particles, confined in the inner allowed region, are called "*trapped particles*", because in a steady state their trajectories do not extend to infinity and thus they remain in the inner allowed region indefinitely.

In 1940, ALFVÉN (1950) proposed the guiding center approximation which with sufficient accuracy greatly simplifies the description of the motions of charged particles in a strong magnetic field. By this approximation, the motion of a charged particle in the inner allowed region is analysed into three parts, namely a circular motion in a plane perpendicular to the magnetic field vector **B** (*the gyration*), a motion along **B** (*the oscillation*), and *a drift motion* along the directions of $\pm\, \mathbf{B} \times \nabla B^2$ and $\pm\, \mathbf{B} \times [(\mathbf{B} \cdot \nabla)\mathbf{B}]$ (the plus sign refers to a positive charge and the minus sign to a negative charge).

The angle between **B** and the velocity vector **w** is called the pitch-angle, here denoted by θ. The pitch-angle θ is related to the intensity of the magnetic field by

$$\sin^2 \theta = \frac{B}{B_0} \sin^2 \theta_0 \,. \tag{1}$$

Thus, the velocity component along the field line, w_s, and the component perpendicular to it, w_n, are given by:

$$w_s = w \cos\theta\,; \qquad w_n = w \sin\theta\,; \qquad w = \sqrt{w_s^2 + w_n^2}\,. \tag{2}$$

At a point where $\theta = \pi/2$ and $B_m = \sin^2\theta/B_o$, w_s becomes zero and a particle is "*reflected back*" towards a weaker field. Such a point is called a mirror point.

To this order of approximation, the motion of a charged particle in a dipole field may be thus expressed: the particle oscillates back and forth with helical motion, between the northern and southern mirror points, and drifts slowly westward or eastward, depending on the sign of its charge.

The velocity $\mathbf{u}$ of the east-west drift motion is given by

$$\mathbf{v} = \mathbf{v}_1 + \mathbf{v}_2\,, \tag{3}$$

and

$$\mathbf{v}_1 = (\tfrac{1}{2}\, m w_n^2 c/eB^4)\, \mathbf{B} \times \nabla B^2/2\,, \tag{4}$$

$$\mathbf{v}_2 = (m w_s^2 c/eB^4)\, \mathbf{B} \times \left[(\mathbf{B}\cdot\nabla)\mathbf{B}\right]. \tag{5}$$

The drift $\mathbf{u}_1$ is caused by inhomogeneity of the magnetic field ($\nabla \mathbf{B}^2$), and the drift $\mathbf{u}_2$ depends on the centrifugal force $m w_s^2/R_c$ associated with the motion along a curved field line. Note that

$$\left| -\mathbf{B} \times \left[\mathbf{B} \times (\mathbf{B}\cdot\nabla)\mathbf{B}\right]/B^2 \right| = B^2/R_c\,. \tag{6}$$

It is worth-while at this point to note that corresponding to the above three motions, the gyration, oscillation and drift motion, there exist three adiabatic invarients (NORTHROP and TELLER, 1960). They are (a) the magnetic moment

$$M = \frac{\frac{1}{2} m w_n^2}{B}$$

of the gyratory motion (b) the longitudinal invariant $I = \int w_s\, \mathrm{d}s$ of the oscillatory motion ($\mathrm{d}s$ = the element of length of the line of force) (c) the third invariant Φ = the magnetic flux through a surface bounded by a magnetic surface (see below). "*Adiabatic*" here means that the above three quantities M, I, Φ change so slowly in a steady state that they may be taken as constants of the motion to a high degree of accuracy (KULSRUD, 1957). The invariance of M has been an important guide for the determination of the characteristics of particle motions in a dipole field. The Equation (1) is simply a direct consequence of this, namely

$$w_n^2/B = w_{no}^2/B_o\,. \tag{7}$$

This equation also gives the change of particle energy due to the betatron acceleration in the non-relativistic case, when $(\mathrm{d}B/\mathrm{d}t)(1/B)$ is much smaller than the frequency of gyration eB/mc.

The longitudinal invariant I makes it possible to define a surface or shell on which the guiding center oscillates and drifts. It is the locus of the lines of force which have the same value of I, and is called a "*magnetic surface*". In a dipole field, because of its axial symmetry, the shell can be generated by rotating the lines of force around the dipole axis. McILWAIN (1961) showed also that it is possible to define magnetic surfaces labeled by a single parameter called L for the actual earth's field.

If the first two invariants are modified in such a way that M is decreased or I is increased, the altitude of the mirror point is reduced; if the reduction is significant, it increases the rate of loss of the particles by collisions in the denser atmosphere. Change in the third invariant signifies the migration of a particle from one magnetic surface to another.

3. Electric Currents

The motions discussed in the previous section, for a group of trapped particles, result in electric current flow of intensity i. We examine how the group characteristics involved in the calculation of the current intensity are related to quantities measured by satellites.

Consider first a group of particles of one kind only, specified by their charge e and mass m. To calculate the current produced in a plasma permeated by a magnetic field, the plasma pressure and the characteristics of the magnetic field must be known at every point in plasma. Let p_s and p_n be the plasma pressure respectively along and perpendicular to $\mathbf{B}$. Let p_m be the magnetic pressure ($= B^2/8\pi$). In terms of p_s, p_n and p_m, together with the vector characteristics of the magnetic field, PARKER (1957) thus expressed the current intensities associated with the above three motions:

(a) The current produced by the gyration $\mathbf{i}_L$

$$\mathbf{i}_L = (c/8\pi p_m)\mathbf{B} \times \{\nabla p_n - \tfrac{1}{2}(p_n/p_m)\nabla p_m - (p_n/p_m)(\mathbf{B}\cdot\nabla)\mathbf{B}/8\pi\}\,. \qquad (8)$$

Within a plasma of uniform pressure ($\nabla p_n = 0$), permeated by a uniform magnetic field ($\nabla p_m = 0$ and $(\mathbf{B}\cdot\nabla)\mathbf{B} = 0$), the current produced by the gyration is exactly cancelled at every point. But any non-uniformity gives rise to a net current. It is expected that in the radiation belt regions the number of trapped particles increases with radial distance to a certain point, and then decreases; this non-uniform distribution will produce a current expressed by the first term in the bracket of Equation (8). If the magnetic field intensity is not uniform, the radius of gyration ($= cmw_n/eB$) and the period of gyration ($= 2\pi cm/eB$) are different at different places, this results in a net current which is expressed by the second term in the bracket. If the lines of force are curved, the circular orbits due to the gyration are more crowded together on the concave side than on the convex side; this results in a net current expressed by the third term in the bracket. Let n be the number of charged particles.

(b) The current produced by the oscillation i_0

$$i_0 = en\,w_s\,.$$

In a steady state, this current is zero, because at any point on the lines of force, the particles passing an area dA (perpendicular to $\mathbf{B}$) on their way to one of the mirror points and on their way back must be equal in number. Because the particles are almost collisionless in the radiation belt regions, they can quickly diminish any electric potential gradient along the field lines. Thus even in a non-steady state, this current intensity may not be significant, and hereafter we neglect this contribution.

(c) The current produced by the drift motion $\mathbf{i}_D$

$$\begin{aligned} \mathbf{i}_D &= en\,(\mathbf{u}_1 + \mathbf{u}_2) \\ &= (c/8\pi p_m)\mathbf{B} \times \{\tfrac{1}{2}(p_n p_m)\,\nabla p_m + (p_s/p_m)(\mathbf{B}\cdot\nabla)\mathbf{B}/8\pi\}\,. \end{aligned} \tag{9}$$

This is due to the two drift motions discussed in § 2. In a uniform magnetic field ($\nabla p_m = 0$), the first term is zero. The second term is zero for particles with the pitch-angle $\theta = \pi/2$ (e.g., trapped particles with the pitch-angle $\theta = \pi/2$ in the equatorial plane do not oscillate ($p_s = 0$), so that their contribution to the second term is null.

(d) The polarization current $\mathbf{i}_p$

$$\mathbf{i}_p = (mnc/B^2)\,\mathbf{B} \times (\mathrm{d}\mathbf{v}/\mathrm{d}t)\,. \tag{10}$$

If the magnetic field intensity is changing, both protons and electrons drift with velocity $\mathbf{v} = c\mathbf{E} \times \mathbf{B}/B^2$ (Note that $c\nabla \times \mathbf{E} = \partial\mathbf{B}/\partial t$). However, because of the difference of their masses, there appears a differential motion between them, resulting in the current denoted by $\mathbf{i}_p$.

The total current is then the combination of (a), (c) and (d), thus;

$$\mathbf{i} = (c/8\pi p_m)\mathbf{B} \times \{\nabla p_n + [(p_s - p_n)/p_m](\mathbf{B}\cdot\nabla)\mathbf{B}/8\pi + mn\mathrm{d}\mathbf{v}/\mathrm{d}t\}\,. \tag{11}$$

The pressure p_s (along $\mathbf{B}$) and p_n (perpendicular to $\mathbf{B}$) are functions of position r (= a radial distance), ϕ (= latitude) and λ (= longitude), and are given by

$$\begin{aligned} p_s\,(r, \phi, \lambda) &= \int\int m w_s^2 n(r, \phi, \lambda, w)\, F(r, \phi, \lambda, \theta, w)\,\mathrm{d}w\,\mathrm{d}\theta \\ p_n\,(r, \phi, \lambda) &= \int\int \tfrac{1}{2} m w_n^2 n(r, \theta, \lambda, w)\, F(r, \theta, \lambda, \theta, w)\,\mathrm{d}w\,\mathrm{d}\theta\,, \end{aligned} \tag{12}$$

where $n(r, \phi, \lambda, w)\,\mathrm{d}w$ = the number density per cm^3 with velocities in the range dw at w at the point (r, ϕ, λ); $F(r, \phi, \lambda, \phi, w)\,\mathrm{d}\theta$ = the fraction of the particles of velocity w with range of the pitch-angle $\mathrm{d}\theta$ at θ at the point (r, ϕ, λ).

It is interesting to see how the functions n and F are related to the quantities measured by instruments carried by satellites (COLEMAN, 1961). All the quantities we deal with here are functions of position; hereafter we omit writing (r, ϕ, λ) unless it is necessary.

Let $j(\theta, \psi, w, t)\,\mathrm{d}A\,\mathrm{d}\Omega\,\mathrm{d}w\,\mathrm{d}t$ denote the number of particles incident, with speed in the range $\mathrm{d}w$ at w, during the time interval at t, from within the solid angle $\mathrm{d}\Omega$ at (θ, ψ = the azimuth angle with respect to $\mathbf{B}$), upon an area $\mathrm{d}A$ normal to the direction of the particle velocity vector $\mathbf{w}$ at a point (r, ϕ, λ). In a steady state ($\partial/\partial t = 0$), assuming axial symmetry, this expression reduces to

$$j(r, \phi, \theta, \psi, w)\, \mathrm{d}A\, \mathrm{d}\Omega\, \mathrm{d}w\,. \tag{13}$$

The omnidirectional intensity $J(w)$, namely the flux of particles with speeds in the range $\mathrm{d}w$ at w, incident from all directions upon a sphere of projected area $\mathrm{d}A$, is

$$J(w) = \left[\int\int j(\theta, \psi, w) \sin\theta\, \mathrm{d}\theta\, \mathrm{d}\psi\right] \mathrm{d}w\, \mathrm{d}A\,. \tag{14}$$

Let $F'(\theta, \psi, w)\, d\Omega$ be the fraction of the particles of velocity w with directions within the solid angle $d\Omega$ at (θ, ψ) at the point (r, ϕ, λ). Then,

$$n(w) F'(\theta, \psi, w)\, w = j(\theta, \psi, w)\,. \tag{15}$$

Hence the omnidirectional intensity may be rewritten as

$$J(w)\, \mathrm{d}w\, \mathrm{d}A = \left[\int\int nF' w \sin\theta\, \mathrm{d}\theta\, \mathrm{d}\psi\right] \mathrm{d}w\, \mathrm{d}A\,. \tag{16}$$

Particle detectors carried by satellites measure J in terms of energy ε, rather than of $w(\varepsilon(\mathrm{Kev}) = \frac{1}{2}mw^2/1.602 \times 10^{-9})$. Further, most of the detectors measure I_o, which is the integrated J for particles with energies larger than ε_m, namely

$$I_o(\varepsilon_m) = \int_{\varepsilon_m}^{\infty} J(\varepsilon)\, \mathrm{d}A\, \mathrm{d}\varepsilon\,. \tag{17}$$

It may be possible to obtain $J(\varepsilon)$ approximately at a given point by using several detectors with different values of ε_m, or by using several detectors each particularly sensitive to a certain energy ε. Further, if F' is measured at the same time, the function $n(w)$ can be obtained from Equation (16).

4. Magnetic Fields Produced by the Ring Current (general); Self-Consistent Solutions and Perturbation Methods

The current Equation (11), enables the ring current field to be calculated. Combined with Maxwell's equation $c\nabla \times \mathbf{B} = 4\pi\, \mathbf{i}$ (neglecting the displacement current) and with the vector equation*

$$[\nabla \times \mathbf{B}]_n = (\mathbf{B}/B^2) \times \{-\tfrac{1}{2}\nabla B^2 + (\mathbf{B} \cdot \nabla)\mathbf{B}\} \tag{18}$$

Equation (11) gives

$$mn \frac{\mathrm{d}\mathbf{v}}{\mathrm{d}t} = -\nabla_n (p_n + p_m) + [(\mathbf{B} \cdot \nabla)\mathbf{B}/4\pi]_n [(1 + (p_n - p_s)/2p_m)]\,. \tag{19}$$

Combining this with

$$\begin{aligned} &\mathrm{div}\,(n\mathbf{v}) + \partial n/\partial t = 0\,, \\ &c\nabla \times \mathbf{E} + \partial \mathbf{B}/\partial t = 0\,, \\ &\mathrm{div}\,\mathbf{B} = 0\,, \\ &\mathrm{div}\,\mathbf{E} = \textstyle\sum en \ (\textstyle\sum = \text{the summation for both protons and electrons})\,, \end{aligned} \tag{20}$$

* $[\,]_n$ signifies a vector component perpendicular to $\mathbf{B}$.

we have a complete set of equations, from which the solution **B** may be obtained when appropriate initial and boundary conditions are given. The solution thus obtained is "*self-consistent*".

Consider the simple case in which the state is steady ($\partial/\partial t = 0$) and div $E = 0$. Then the set reduces to

$$\nabla_n(p_n + p_m) = [(\mathbf{B} \cdot \nabla)\mathbf{B}/4\pi]_n(1 + (p_n - p_s)/2p_m) \; ; \; \text{div } \mathbf{B} = 0 \, . \tag{21}$$

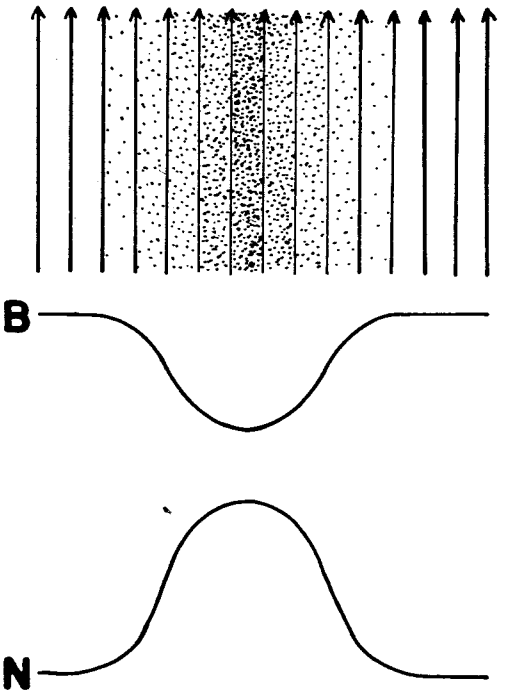

Fig. 4. The schematic diagram to show the distribution of the field intensity B in a cylindrical plasma. The distribution of plasma is given by N.

If also the plasma is confined in a uniform magnetic field (its field lines being parallel to the axis of cylinder, so that $(\mathbf{B} \cdot \nabla)\mathbf{B} = 0$) and if the plasma particles move wholly in planes perpendicular to **B**(so that $p_s = 0$), then,

$$p_n + p_m = p_n + \frac{B^2}{8\pi} = \frac{B_o^2}{8\pi} \, . \tag{22}$$

Here B_0 denotes the field intensity outside the cylindrical plasma, and B is the self-consistent solution for this particular case. Figure 4 shows this situation schematically. In this case, the decrease of the field intensity in the plasma cylinder is entirely due to the current i_L, and thus it is said to be due to the "*diamagnetism*" of the plasma.

Unfortunately there is no simple way of obtaining such a self-consistent solution for a group of trapped particles confined in a dipole field. The deformation of the earth's field due to the trapped particles affects their motions and thus the current intensity and the magnetic field; thus it is a non-linear problem.

A first approximation is obtained by assuming that the magnetic field produced by the particles does not affect their motions. In our dipole case, this means that the field intensity F_1 at a given point is simply the sum of the ring current field $\nabla_1 F$ and the earth's dipole field F_E,

$$F_1 = F_E + \nabla_1 F . \tag{23}$$

A second approximation ($\nabla_2 F$) to the ring current field is then obtained by supposing the particles to move in the field F_1: this gives the new estimate F_2 for the total field:

$$F_2 = F_E + \nabla_2 F . \tag{24}$$

In principle, such a process can be continued to any order of approximation (namely, $F_n = F_E + \nabla_n F$), and if F_n converges rapidly to a certain value, it may be close to a self-consistent solution.

5. First Approximation

A. GROUP CHARACTERISTIC FUNCTIONS

The expression (11) for the current intensity **i** involves p_s and p_n, each of which depends on a product of two "*group characteristic functions*" $n(r, \phi, \lambda; w)$ and $F(r, \phi, \lambda; \theta; w)$. Hereafter, to show the essence of the calculation, we consider particles with speeds between w and $w + \mathrm{d}w$ only; also F is assumed to be a function of θ only, namely

$$\begin{aligned} &n\,\mathrm{d}w = n(r, \phi; w)\,\mathrm{d}w \;(= \text{the number density distribution function}) , \\ &F = F(\theta) = F' \;(= \text{the pitch-angle distribution function}) . \end{aligned} \tag{25}$$

This implies an axial symmetry ($\partial/\partial\lambda = 0$). By suitable integrations the results can be extended to the case when the particles have different speeds w and F is a function of w and position.

It has been noted that for a group of trapped particles, $F(\theta)$ has a form of $\sin^{\alpha+1}\theta$. It is shown later that this form of $F(\theta)$ can express fairly well observed $F(\theta)$. We note that $F(\theta)$ must satisfy (cf. PARKER, 1957)

$$\int_0^{\pi} F(\theta)\,\mathrm{d}\theta = 1 , \tag{26}$$

so that

$$\begin{aligned} &F(\theta) = A(\alpha)\sin^{\alpha+1}\theta , \\ &A(\alpha) = \Gamma(\alpha + 2)/2^{\alpha+1}\{\Gamma(\tfrac{1}{2}\alpha + 1)\}^2 . \end{aligned} \tag{27}$$

If $\alpha = 0$, $F(\theta) = \frac{1}{2}\sin\theta$, and the pitch-angle distribution is said to be isotropic.

Figure 5 shows $F(\theta)$ for $\alpha = 0$, -0.9 and 2.0. For $\alpha > 0$, large pitch angles are in excess, for $\alpha < 0$, the smaller pitch-angles.
Introducing (27) into (12), we have

$$\begin{aligned} p_s &= \int m w_s^2 n F(\theta)\, \mathrm{d}\theta\, \mathrm{d}w \\ &= m w^2 n \int F(\theta) \cos^2\theta\, \mathrm{d}\theta\, \mathrm{d}w \\ &= m w^2 n (1 - 4B(\alpha))\, \mathrm{d}w\,, \\ p_n &= \int \tfrac{1}{2} m w_n^2 \mathrm{F}(\theta)\, \mathrm{d}\theta\, \mathrm{d}w \\ &= m w_n^2 \int \mathrm{F}(\theta) \sin^2\theta\, \mathrm{d}\theta\, \mathrm{d}w \\ &= 2 m w^2 n B(\alpha)\, \mathrm{d}w\,, \end{aligned} \tag{28}$$

where

$$B(\alpha) = (\alpha + 2)/4(\alpha + 3)\,.$$

For the pitch-angle distribution given by Equation (27), the relation between n at a general point and n_0 at its associated point P_0 on the same line of force, is given by

$$n = n_0 (B_0/B)^{\alpha/2}\,, \tag{29}$$

where B_0 and B are the field intensities at P_0 and P, respectively. Therefore, in a dipole field, in which B_e/B is a known function, the number density n is determined at every point by α and by the number density along an equatorial radius r_e. (The suffix e signifies values in the equator plane).

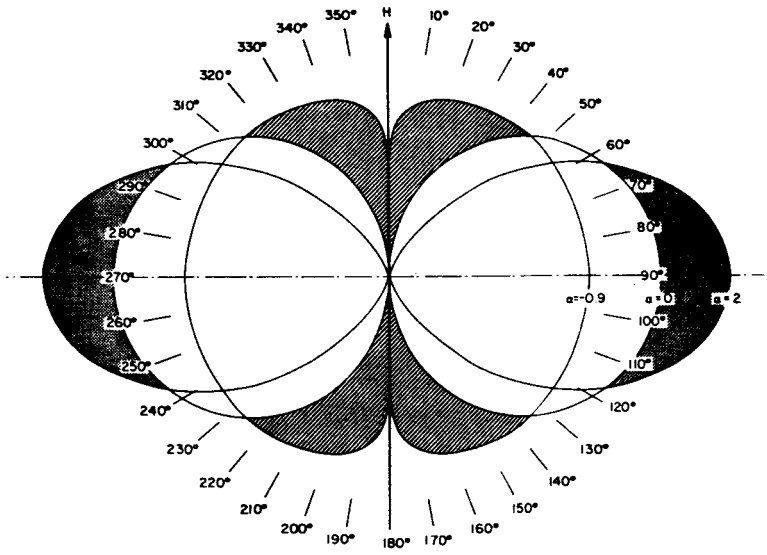

Fig. 5. The pitch-angle distribution $F \sim \sin^{\alpha+1}\theta$ for $\alpha = 2.0$, 0, and -0.9. The deviation from the isotropic distribution ($\alpha = 0$) is shown by a dotted area for $\alpha = 2$ and by a hatched area for $\alpha = -0.9$.

We find that n along an equatorial radius (or in the equatorial plane) can be reasonably represented by

$$\begin{aligned} n &= n_o e^{-g_1^2 z^2} \ (z < 0\text{: the inner part of the belt}) , \\ n &= n_o e^{-g_2^2 z^2} \ (z > 0\text{: the outer part of the belt}) , \end{aligned} \tag{30}$$

where

$$z = (r_e - r_{eo})/a; \ \ a = \text{the earth radius} .$$

Here r_{eo} denotes the radial distance of the point at which n attains its maximum value n_o. These equations, together with (29), determine the number density at any point (r, ϕ) in a given magnetic field in terms of n_o, r_{eo}, g_1, g_2 and α.

B. DIPOLE FIELD

In our first approximation, it is assumed that trapped particles move in an unperturbed dipole field. The position of any point P in a dipole field will be specified by usual spherical polar coordinates or by (r_e, ϕ, λ), where r_e denotes the radial distance of the related point P_e where the dipole field line through P crosses the equatorial plane. In this section, the latter system is found to be more convenient.

With each point P we associate two unit vectors $\mathbf{j}$, $\mathbf{k}$ which with $\mathbf{h}$, the unit vector $\mathbf{B}/B$ along B, form a right-handed orthogonal unit vector triad; $\mathbf{k}$ is the eastward unit vector normal to the meridian plane through P and $\mathbf{j}$ is the unit vector $\mathbf{k} \times \mathbf{h}$: it is outward from the origin (but not radially outward). Let P' be a point adjacent to P with coordinates differing by dr_e, $d\phi$ and $d\lambda$ from those of P, namely r_e, ϕ, λ. The vector element PP' or $\mathbf{ds}$ can be specified as follows relative to the vector triad $\mathbf{h}, \mathbf{j}, \mathbf{k}$,

$$\mathbf{ds} = \mathbf{h} h_1 \mathrm{d}\phi + \mathbf{j} h_2 \mathrm{d}r_e + \mathbf{k} h_3 \mathrm{d}\lambda .$$

Here

$$\begin{aligned} h_1 &= r_e (1 + 3 \sin^2 \phi)^{\frac{1}{4}} \cos \phi \\ h_2 &= \cos^3 \phi / (1 + 3 \sin^2 \phi)^{\frac{1}{2}} \\ h^3 &= r_e \cos^3 \phi . \end{aligned} \tag{31}$$

Hence an element of area $\mathrm{d}S_3$ in the meridian plane through P, bounded by the lines of force, r_e and $r_e + dr_e$, and the radii ϕ and $\phi + \mathrm{d}\phi$, is given by

$$\begin{aligned} \mathrm{d}S_3 &= h_1 h_2 \, \mathrm{d}r_e \mathrm{d}\phi \\ &= r_e \cos^4 \phi \, \mathrm{d}r_e \, \mathrm{d}\phi . \end{aligned} \tag{32}$$

Further, since the tubes of magnetic force are of constant strength,

$$B h_2 h_3 = (B h_2 h_3)_e ,$$

where the suffix e signifies reference to the equatorial point on the field line through P,

Hence

$$B_e/B = h_2 \cos^3 \phi \,, \tag{33}$$

$$B_e = a^3 B_o / r_e^3 \,, \tag{34}$$

$B_o = 0.32$ gauss $= B_e$ at the equator at the earth's surface .

A volume element $\mathrm{d}V$ at P can similarly be expressed by

$$\begin{aligned} \mathrm{d}V &= h_1 h_2 h_3 \, \mathrm{d}r_e \, \mathrm{d}\phi \, \mathrm{d}\lambda \\ &= r_e^2 \cos^7 \phi \, \mathrm{d}r_e \, \mathrm{d}\phi \, \mathrm{d}\lambda \,. \end{aligned} \tag{35}$$

The gradient of a scalar function Q in our coordinate system is given by

$$Q = \mathbf{h} \frac{1}{h_1} \frac{\partial Q}{\partial \phi} + \mathbf{j} \frac{1}{h_2} \frac{\partial Q}{\partial r_e} + \mathbf{k} \frac{1}{h_3} \frac{\partial Q}{\partial \lambda} \,.$$

If the system is axially symmetric, the last term in the above equation is zero, and

$$\mathbf{h} \times \nabla Q = \frac{1}{h_2} \frac{\partial Q}{\partial r_e} \mathbf{k} \,. \tag{36}$$

Note also that the radius of curvature R_c is given by

$$\frac{1}{R_c} = \frac{3(1 + \sin^2 \phi)}{r_e \cos \phi (1 + 3 \sin^2 \phi)^{\frac{1}{2}}} \,. \tag{37}$$

C. THE V_3 BELT

The V_3 belt, originally proposed as a model ring current belt by AKASOFU and CHAPMAN (1961), has later been extensively studied by AKASOFU, CAIN and CHAPMAN (1961). This model can serve for some semi-quantitative discussions on the general features of the magnetic field produced by a group of trapped particles.

The model belt is assumed to consist of protons of energy 150 kev. (The current would be the same if it consisted of electrons of the same energy; see (28)). The radial distance r_{eo} of the point at which n attains the maximum value $n_o = 1/\mathrm{cm}^3$ is taken to be $6a$. The distribution of the particles around r_{eo} is chosen so that n is reduced by a factor of 10 at the distance $\pm a$ from r_{eo}. The pitch-angle distribution is assumed to be anisotropic with $\alpha = -0.5$. Further, a steady state is assumed throughout. Thus the parameters are

$$\begin{aligned} r_{eo} &= 6a, && (r_{eo}/a = f_o) \\ n_0 &= 1.0/\mathrm{cm}^3 \\ g_1 &= g_2 = g = 1.517 \\ \alpha &= -0.5 \\ \varepsilon &= 150 \text{ kev} && (n_0 \varepsilon = 150 \text{ kev/cm}^3) \,. \end{aligned} \tag{38}$$

The current intensity vector **i** in (11) is now given by

$$i = \frac{c}{BR_c}(p_s - p_n) - \frac{c}{Bh_2}\left(\frac{\partial p_n}{\partial r_e}\right). \tag{39}$$

$$\mathbf{i} = -\mathbf{k}i,$$

Using Equations (36) and (37), Equation (39) is now rewritten thus:

$$i = \frac{mcn_0w^2\,\mathrm{d}w}{B_0a}\{(f_0 + z)^2\,\mathrm{e}^{-g^2z^2}D(\phi, \alpha) + 2g^2z(f_0 + z)^3\,\mathrm{e}^{-g^2z^2}F(\phi, \alpha)\}. \tag{40}$$

Here

$$D(\phi, \alpha) = \frac{3\{1 - 6B(\alpha)\}(\cos\phi)^{5+3\alpha}(1 + \sin^2\phi)}{(1 + 3\sin^2\phi)^{2+\frac{1}{2}\alpha}},$$

$$F(\phi, \alpha) = \frac{2B(\alpha)(\cos\phi)^{3\alpha+3}}{(1 + 3\sin^2\phi)^{\frac{1}{2}\alpha}}.$$

The calculated values of i thus obtained have been used to draw lines of constant current intensity in a meridian plane in Figure 6. The full lines indicate westward current, the broken lines eastward current; the current intensity at r_{eo} is taken to be unity.

Let Δ_1F_x and Δ_1F_z denote respectively the components of the magnetic field of the ring current, based on the first approximation, parallel and perpendicular to the

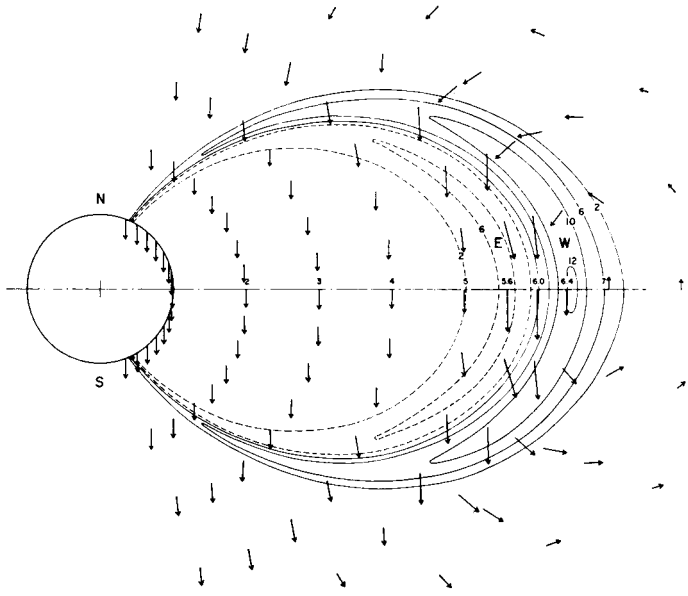

Fig. 6. The field vectors of Δ_1F, the first approximation to the magnetic field of the V_3 belt.

equatorial plane at the point (r_{e1}, ϕ_1). Let δF_x and δF_z denote the contributions to these components, made by the part of the ring current i that flows across the section dS_3 at the point (r_{e2}, ϕ_2). They are given (cf. STRATTON, 1941; p. 263) by

$$\delta F_x = -\frac{2i\,dS_3}{c}\frac{\zeta}{\varpi\left[(\xi+\varpi)^2+\zeta^2\right]^{\frac{1}{2}}}\left[-K+\frac{\xi^2+\varpi^2+\zeta^2}{(\xi-\varpi)^2+\zeta^2}E\right],$$
$$\delta F_z = -\frac{2i\,dS_3}{c}\frac{1}{\left[(\xi+\varpi)^2+\zeta^2\right]^{\frac{1}{2}}}\left[K+\frac{\xi^2-\varpi^2-\zeta^2}{(\xi-\varpi)^2+\zeta^2}E\right], \tag{41}$$

where

$$\varpi = r_{e1}\cos^3\phi_1\,,$$
$$\zeta = r_{e1}\cos^2\phi_1\sin\phi_1 - r_{e2}\cos^2\phi_2\sin\phi_2\,,$$
$$\xi = r_{e2}\cos^3\phi_2\,,$$

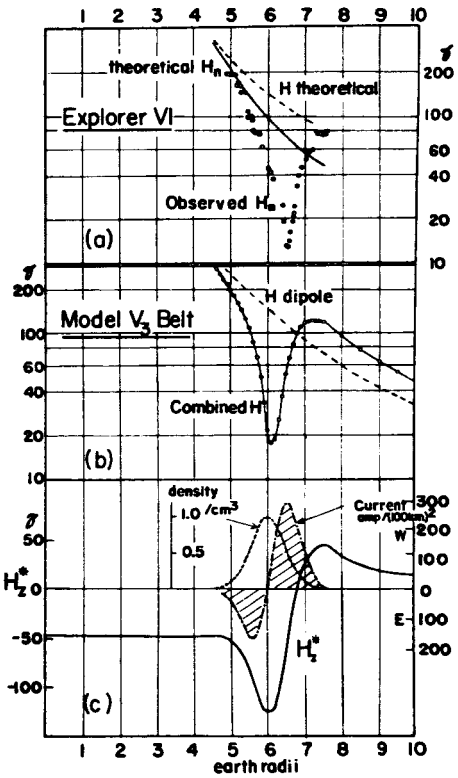

Fig. 7. (a) The magnetic field measurements made by the magnetometer carried on Explorer VI (SMITH, COLEMAN, JUDGE and SONETT, 1960). (b) The field distortion produced in the equatorial plane by the V_3 belt. (c) The number density distribution, and the corresponding distribution of current intensity and magnetic field intensity for the equatorial plane. ($H_z = \Delta_1 F_z$).

and $K(k^2)$ and $E(k^2)$ are the complete elliptic integrals of the first and second kinds for

$$k^2 = \frac{4\xi\varpi}{(\xi + \varpi)^2 + \zeta^2} .$$

Thus,

$$\begin{aligned} \Delta_1 F_x &= \int \delta F_x \, \mathrm{d}S_3 , \\ \Delta_1 F_z &= \int \delta F_z \, \mathrm{d}S_3 . \end{aligned} \tag{42}$$

The above integration was replaced by a double summation which was made by IBM 704 and IBM 7090 Computers, for 924 elements $\mathrm{d}S_3$ of the meridian cross-section of the belt. Figure 6 shows the distribution of the field vectors, of magnitude

$$\Delta_1 F = \sqrt{\Delta_1 F_x^2 + \Delta_1 F_z^2}$$

together with the contours of the current intensity distribution. Note that since this is the first approximation, the vector scale of force is simply proportional to the energy density at r_{eo}, namely $n_o\varepsilon$ kev/cm^3.

Clearly the field $\Delta_1 F$ is fairly uniform within a radius of about $2a$, and is almost parallel to the dipole axis, agreeing with the observed Dst field during magnetic storms. Beyond this distance, $\Delta_1 F$ becomes notably non-uniform; it shows considerable curl in the region of most intense current. Outside the belt, the field tends, with increasing distance, to similarity with a dipole field.

Figure 7c shows the number density distribution $n(r_e)$, the current intensity distribution $i(r_e)$ in the equatorial plane, and the ring current field intensity in the equatorial plane $\Delta_1 F_z(r_e)$; note that $\Delta_1 F_x = 0$ in the equatorial plane. In this first approximation, the resulting field is a linear combination of the field $\Delta_1 F$ with the earth's dipole field F_E. For comparison, Figure 7a shows the magnetic field measurements made by the magnetometer carried by Explorer VI.

The significant dip around $r_{eo} = 6a$ is mainly due to the diamagnetism discussed in Section 4. However, the contribution from the drift current i_D becomes increasingly important with increase of distance from r_{eo}. At the earth's surface (at the equator), the contributions from i_L and i_D are respectively $+ 11.2\gamma$ and $- 56.6\gamma$, so that the total change is $- 45.4\gamma$. There the contribution from i_L is positive, and the major contribution to the Dst decrease comes from the drift current i_D.

Figures 8a and 8b show $\Delta_1 F_x$ and $\Delta_1 F_z$, together with $F_1 = F_E + \Delta_1 F$ along radii $\phi = 20°$ and $\phi = 40°$. The dip seen in the F_1 curve for the equatorial radius is less prominent at higher latitudes. Thus in order to study the magnetic effects of trapped particles, satellites should orbit lie close to the equatorial plane.

Figure 9 shows the distortion produced by the ring current belt in the field lines, there compared with those of the dipole. The "*anchoring points*" where the lines cross the earth's surface do not change appreciably; but the ring current stretches the lines.

D. THE QUIET-TIME PROTON BELT

Recent observations by the Explorer XII satellite have revealed an extensive belt of

protons of low energy (between 150 kev and 4.5 Mev) (DAVIS and WILLIAMSON, 1962). Figure 10 (top) shows a typical equatorial flux distribution during magnetically quiet conditions, as a function of radial distance from the earth's center; it is based on

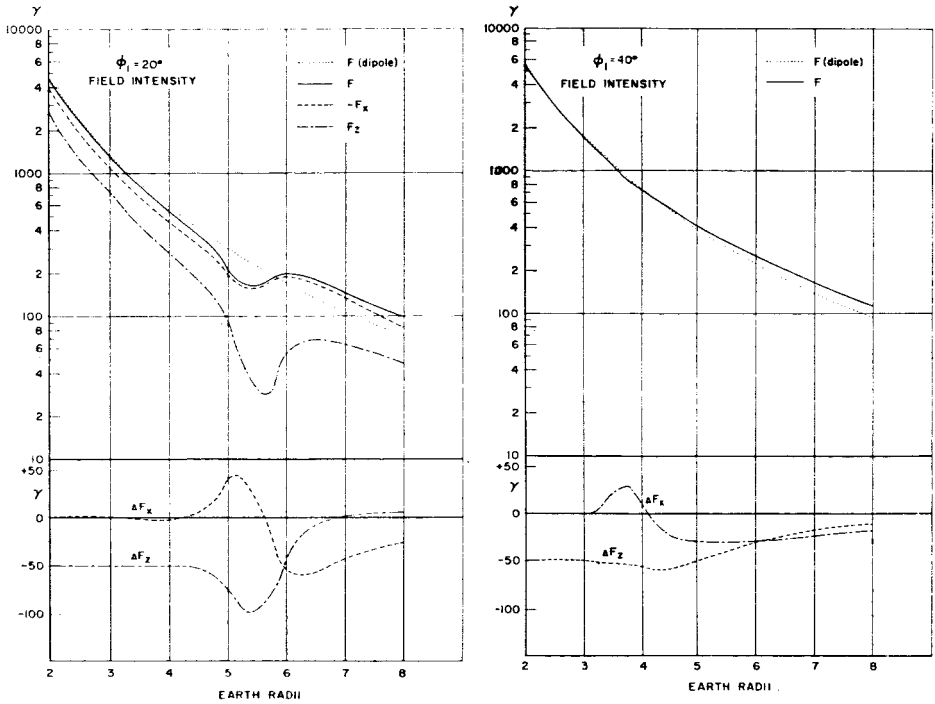

Fig. 8. (a) and (b): The upper parts consist of graphs, on a logarithmic scale, of the intensity of the dipole field F_E and of F_1 along radii $\theta = 20°$ and 40°, respectively. The lower parts show the x and z component of $\Delta_1 F$.

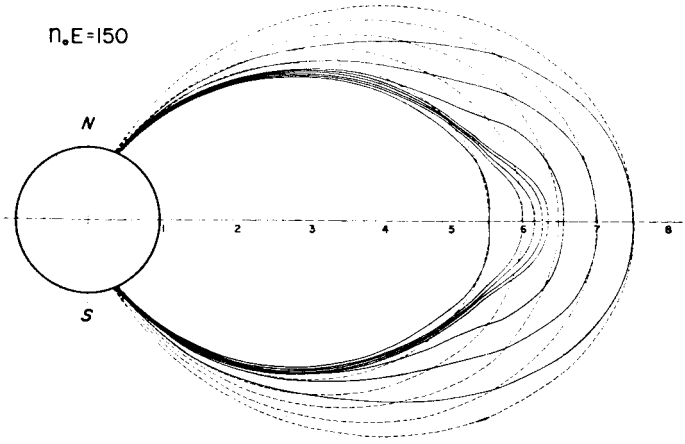

Fig. 9. The lines of forces of F_1, the first approximation to the combined field of the geomagnetic dipole and the V_3 belt.

one of the paths of Explorer XII, that lay close to the equatorial plane beyond $r = 3.5a$.

The number density distribution of the observed proton belt can be approximately represented by Equation (30), with the parameters $r_{eo} = 3.2a$, $g_1 = 2.990$, $g_2 = 0.419$, $n_o\varepsilon = 300$ kev/cm^3 (e.g., $n_o = 0.6$/cm^3, $\varepsilon = 500$ kev) (see Figure 10, bottom). For simplicity the belt is treated as consisting of mono-energetic protons (500 kev). The energy spectrum, however, becomes steeper for larger r_e, indicating a relative increase

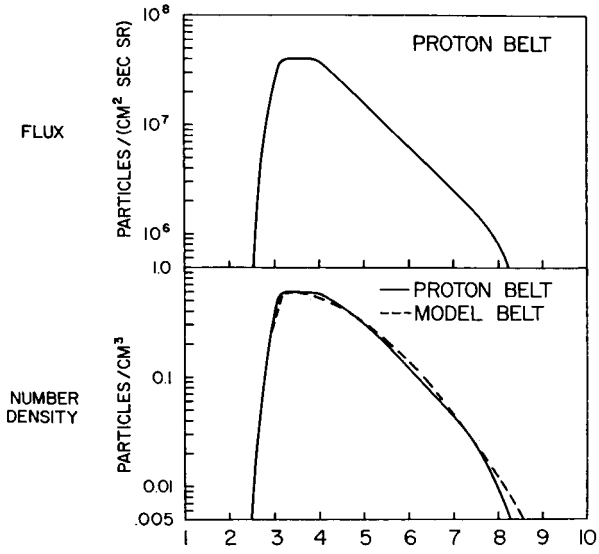

Fig. 10. (Top) A typical equatorial flux distribution in the proton belt, as a function of radial distance from the earth's center. (Bottom) The number density distribution in the model belt and in the observed proton belt.

of lower energy protons with increasing geocentric distance. The calculation of the current and field can be extended to such a more complicated actual case without much difficulty, by repeating the procedure for each spectral component, and finally summing the contributions.

DAVIS and WILLIAMSON also measured the pitch-angle distribution $F(\theta)$, shown in Figure 11. The curve for $F(\theta) \sim \sin^3 \theta$ (namely, $\alpha = 2.0$) there also shown, agrees reasonably well the observed one. Altogether, the necessary parameters are:

$$r_{eo} = 3.2a$$
$$g_1 = 2.990$$
$$g_2 = 0.419$$
$$\alpha = 2.0$$
$$n_o\varepsilon = 300 \text{ kev/cm}^3 .$$

Figure 12 (bottom) shows the graph of $\Delta_1 F_z$ along an equatorial radius for these values of the five parameters r_{eo}, g_1, g_2, α and n_o. The intensity has a minimum value of about $-$ 72 γ at $r_e = 4.1\ a$ and a maximum value of about $+$ 21 γ at $r_e = 8.0\ a$. The corresponding field at the earth's surface is about $-$ 38 γ. This is less than 0.2% of B_o ($= 0.32$ gauss). Figure 12 (top) gives the combined field $F_1 = F_E + \Delta_1 F$.

Perhaps the most significant feature of this particular example, based on an actually observed belt, is that it has the largest magnetic effect of all the belts dis-

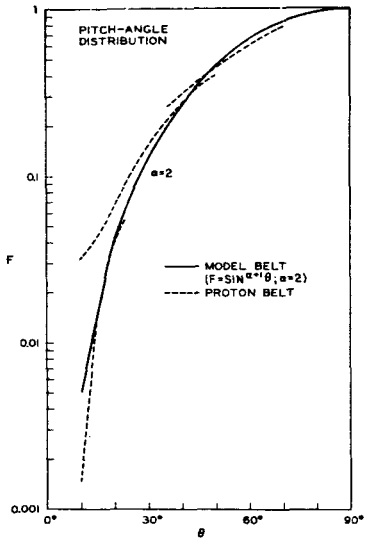

Fig. 11. The pitch-angle distribution in the model belt, together with measured one.

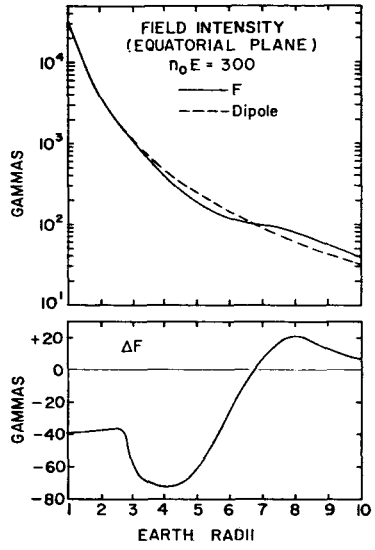

Fig. 12. (Top) The distortion of the earth's dipole field produced by the model belt in the equatorial plane. (Bottom) The distribution of the magnetic field $\Delta_1 F$ produced by the model proton belt in the equatorial plane.

covered so far. We show later that this proton belt may well be identified with what has been called the "*quiet-time ring current*", particularly by cosmic ray physicists. Further, the growth and decay of this belt seem to be closely related to the storm-time ring current belt. This is discussed later in detail (Section 9).

6. The Second Approximation

Observation and calculation both show that a group of trapped particles can significantly distort the earth's dipole field. This distortion, in turn, affects the motions of the particles, and thus the resulting current intensity i and the magnetic field produced. Hence our calculation of $\Delta_1 F$, the first approximation to the ring current field, needs correction.

Our general procedure here is to calculate first $\Delta_1 F$ for a small value of $n_o\varepsilon$ in such a way that $F_E \gg \Delta_1 F$. Then, the lines of force must be calculated for $F_1 = F_E + \Delta_1 F$.

Then the number density $n(r_e, \phi), p_s, p_n, R_c$ and other necessary quantities may be calculated along the lines. However, we no longer have simple relations such as (33) and (37), so that a large amount of numerical calculation is required, in addition to the double summation for the magnetic field calculation.

In a paper by AKASOFU, CAIN and CHAPMAN (1961), $\Delta_2 F$ was calculated for such an example of the V_3 belt ($g_1 = g_2 = 1.517$; $\alpha = -0.5$) with $n_o\varepsilon = 90$ kev/cm^3. The

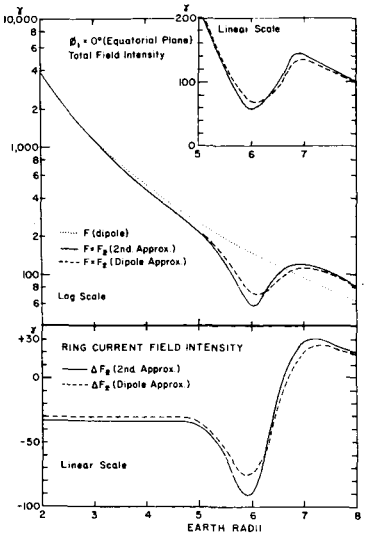

Fig. 13. (Top) The distortion of the earth's dipole field F_2 produced by the V_3 belt, together with F_1 and the dipole. (Bottom) The distribution of the magnetic field $\Delta_1 F$ and $\Delta_2 F$ produced by the V_3 in the equatorial plane.

results are presented in Figure 13. It shows that the second approximation corrects $\Delta_1 F$ around the center line of the belt ($r = r_{eo}$) by a maximum amount of 15 γ. The change from $\Delta_1 F$ to $\Delta_2 F$ scarcely alters the location where $\Delta_1 F$ is most intense, but it deepens this minimum by about 15γ. Except in this region, the correction for the second approximation is less than 10γ; at the earth's surface, the correction does not exceed 3γ (10% of $\Delta_1 F$).

It is not definitely known whether F_n thus successively obtained would approach a limiting value F. The calculation of $\Delta_3 F$ or of any higher ones has not been attempted yet.

During the growth or decay stage of the ring current there will be an electric field associated with the changing magnetic field:

$$\partial \mathbf{B}/\partial t = -(1c)\nabla \times \mathbf{E}\,.$$

Such an electric field will modify the mass motion and distribution of the ring current particles (of velocity $\mathbf{v} = (1/c)\,\mathbf{E} \times \mathbf{B}$), considerably complicating our problem.

7. The Magnetic Moment of the Ring Current

The magnetic moment M_R of the ring current is given by

$$M_R = \frac{\pi a^2}{c} \int i(r_e, \phi) f_e^2 \cos^6\phi \, dS_3 , \tag{44}$$

where

$$f_e = r_e/a$$

$$dS_3 = a^2 f_e \cos^4\phi \, d f_e \, d\phi .$$

For our model ring current belt, $i(r_e, \phi)$ can be obtained if the parameters r_{eo}, g_1, g_2, α, $n_o\varepsilon$ are given. In our first approximation M_R is proportional to $n_o\varepsilon$, hence we may write

$$\begin{aligned} M_R &= \Delta m n_o \varepsilon , \\ \Delta m &= m'(r_{eo}, g_1, g_2, \alpha) \\ &= 1.62 \times 10^{19} \{(A_1 + A_2) I_D' + (B_1 + B_2) I_F'\} . \end{aligned} \tag{45}$$

Here A_i and B_i are given by

$$A_i = \frac{\sqrt{\pi}}{2} \; X_i \pm \; 5Y_i \pm \frac{1}{g_i^6}$$

$$B_i = 3\sqrt{\pi}\, X_i \pm 30 Y_i \pm \frac{6}{g_i^6} ,$$

where the minus sign refers to $i = 1$ and the plus sign to $i = 2$. In terms of the numbers X_i, Y_i, and f_o thus defined,

$$X_i = \frac{f_o^5}{g_i} + \frac{5 f_o^3}{g_i^3} + \frac{15 f_o}{4 g_i^5}$$

$$Y_i = \left(\frac{f_o^2}{g_i^2}\right)\left(\frac{f_o^2}{2} + \frac{1}{g_i^2}\right)$$

$$f_o = r_{eo}/a .$$

$$(i = 1, 2)$$

Further,

$$I_{D'} = 3 \{1 - 6B(\alpha)\} \int_0^{\pi/2} \frac{(1 + \sin^2\phi)(\cos\phi)^{15+\alpha}}{(1 + 3\sin^2\phi)^{2 + \frac{1}{2}\alpha}} \, d\phi$$

For $\alpha = 2.0$

$$I_{D'} = -0.1267$$

$$I_{F'} = \quad 0.1036.$$

The same set of parameters determines also the magnetic field produced by the ring current. Let $\Delta_1 F_s$ denote $\Delta_1 F$ at the equator at the earth's surface.

Both M_R and $\Delta_1 F_s$ are proportional to $n_0\varepsilon$ in our first approximation, but our approximation breaks down when $n_0\varepsilon$ reaches the value for which at some point within the belt $\Delta_1 F$ approaches the dipole field intensity F_E there; the calculated field intensity

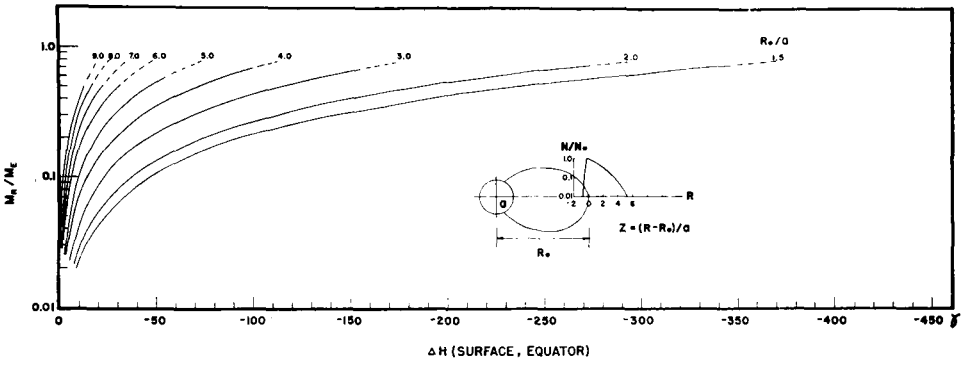

Fig. 14. The ratio (M_R/M_E) of the magnetic moment of model ring current belts to that of the earth plotted against the ring current fields at the equator at the earth's surface.

F would become zero at that point. At present, unfortunately, there is no simple way of determining M_R and $\Delta_1 F$ in a self-consistent way when the field distortion due to the ring current becomes serious for a large value of $n_0\varepsilon$. Because a further increase of $n_0\varepsilon$ beyond such a critical value would not much increase M_R and $\Delta_1 F$, we may take the critical value to be an approximate upper limit for $n_0\varepsilon$. This critical value will differ for different types of the belt.

To examine this point, we choose the set of the parameters $g_1 = 2.990$, $g_2 = 0.419$ and $\alpha = 2.0$, together with several different values of r_{eo} (these values of g_1, g_2 and α are the same as those for the quiet-time proton belt). Figure 14 shows for several values of r_{eo}/a the relation between the ratio M_R/M_E (M_E = the magnetic moment of the earth = 8.1×10^{25} gauss cm^3) and $\Delta_1 F_s$ (the ring current field at the equator at the earth's surface). The enhancement of $n_0\varepsilon$ increases both M_R/M_E and $\Delta_1 F_s$, as is indicated by each r_{eo}/a curve, although the values of $n_0\varepsilon$ do not appear explicitly in the Figure. The termination of the solid part in each curve indicates the approximate upper limits of M_R/M_E and $\Delta_1 F_s$ for each belt.

Figure 15 shows also $\Delta_1 F/n_0\varepsilon$ as a function of r over the range from 3.5 to 6.0 (AKASOFU and CAIN, 1962). Clearly the magnetic "*efficiency*" of the particles (per unit $n_0\varepsilon$) increases with r_{eo}. However, since F_E decreases rapidly with r_{eo}, the critical

value of $n_o\varepsilon$ decreases with increasing geocentric distance. As a result, the maximum $\Delta_1 F_s$ is larger for smaller r_{eo}.

As Figure 14 shows, the ratio M_R/M_E is less than unity for all values of r_{eo}/a. This conclusion is particularly important for cosmic ray physicists. Assuming that both the earth's dipole field and the ring current field extend to infinity, the ring current reduces

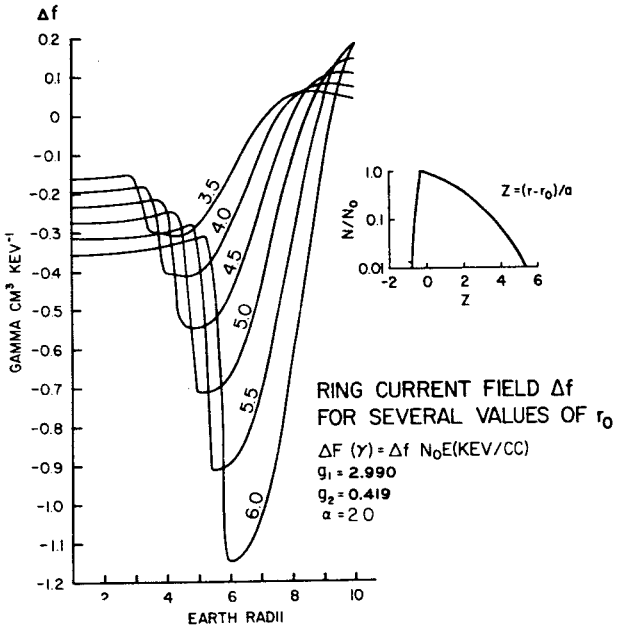

Fig. 15. The distribution of the magnetic field $\Delta_1 F/n_o\varepsilon$ for the same set of parameters g_1, g_2 and α, but different values of r_{eo}.

STÖRMER's cut-off rigidity P_o for solar protons approaching to the polar ionosphere to (KELLOGG and WINCKLER, 1961)

$$P = \frac{P_o}{1 + \frac{M_R}{M_E}}. \tag{46}$$

Because the ratio M_R/M_E is not likely to be more than unity,

$$P > P_o/2\,.$$

At College (Alaska), where $P_o = 0.48$ Gv, the lowest value of P due to the ring current is then 0.24 Gv, corresponding to a solar proton energy of order 60 Mev. However, protons of energy 0.5 Mev ($P = 0.031$ Gv) have been observed during magnetic storms at about the same geomagnetic latitude. This suggests that the observed reduction is not wholly due to the ring current, or that the ring current cannot much

reduce P if it is acting alone. The same conclusion may be applied to the quiet-time ring current, namely the quiet-time proton belt, because the maximum ratio expected is of order 0.63.

8. Deformations of the Outer Radiation Belt

A. LOWERING OF THE BOUNDARY L VALUE

Recent improved measurements by satellites, especially Explorer XII and Injun I, have revealed an extensive low-energy electron belt ($\sim$ 40 kev) as well as the proton belt (the quiet-time proton belt). Both satellites showed also a rather sharp outer boundary, beyond which there is no significant flux of such electrons. Figure 16a shows this situation schematically, together with a typical Injun I observation (Figure 16b).

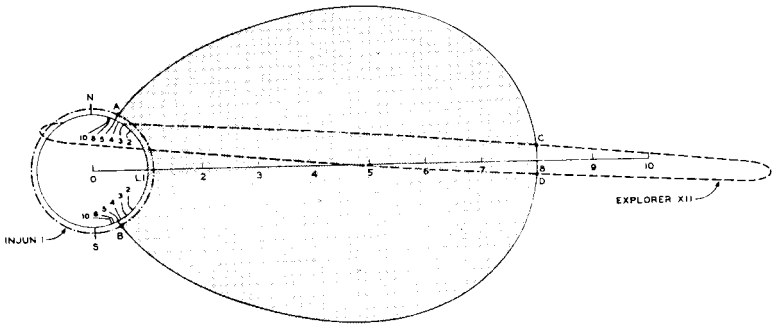

Fig. 16a. The schematic diagram to show the orbits of the Injun I and Explorer XII satellites with respect to the outer radiation belt.

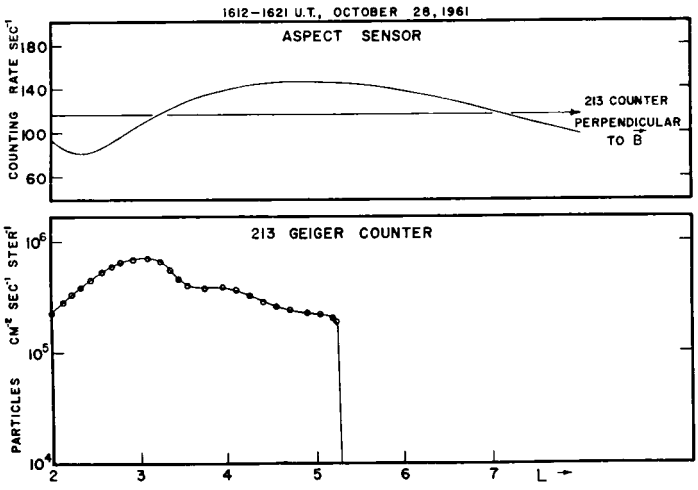

Fig. 16b. The typical latitudinal variation of the directional flux of electrons of greater than 40 kev energy during geomagnetically disturbed conditions in October 1961. (MAEHLUM and O'BRIEN, 1963).

One conventional way of visualizing the distortion of the earth's magnetic field is to find the distorted field lines or deformed magnetic L surfaces and to compare them with those calculated from the potential function obtained by spherical harmonic analysis of the earth's field at the earth's surface. This cannot be done in a simple way by having two or three simultaneous satellites with magnetometers. However, because trapped particles move on the magnetic L surfaces, some distinct features of their distribution in space obtained simultaneously by two or more satellites, offer a useful guide for this purpose.

In Figure 16, if the earth's magnetic field is expressed by the scalar potential function, the outer boundary must coincide with one of the calculated magnetic L surfaces, corresponding to a certain value of L (McIlwain, 1961), say $L = 8.0$. Thus, the boundary L values observed by the two satellites, at the points A, B, C, and D, must be the same. Maehlum and O'Brien (1963) suggest, however, that in general the boundary L values obtained by the two satellites do not agree. Such a discrepancy seems to become serious during the main phase of an intense magnetic storm. A boundary L value as small as 4.0 was observed by Injun I during the main phase of the October 28, 1961 magnetic storm: however, the minimum boundary L value obtained by Explorer XII during its life time was around $L \approx 8.0$ (Freeman, Van Allen and Akasofu, to be published). This strongly suggests that the earth's magnetic field and the magnetic L surfaces containing such low energy electrons are sometimes greatly distorted, particularly during the main phase of magnetic storms. Therefore, it is interesting to examine if model ring currents, such as those proposed earlier, can explain the observed deformation of the outer radiation belt. We note in this respect that although the ring current can seriously distort the earth's field in the radiation belt regions, its effect at the earth's surface is in general of order 1% of the permanent field, which is within the uncertainty of the present spherical harmonic analysis ($\pm$ 1%). We know now also that the earth's magnetic field does not extend to infinity and that it is confined in a cavity bounded by solar plasma. The effect of this limitation at the earth's surface is a worldwide ("*DCF*") increase of the horizontal component of the earth's field, in general by not more than $+100\ \gamma$ of order--- only 0.3% of the permanent field. This again is within the uncertainty of the spherical harmonic analysis.

For the model ring current, we take the following parameters

$$r_{eo} = 3.0a$$
$$g_1 = 2.990$$
$$g_2 = 0.419$$
$$\alpha = 2.0 \quad .$$

Several values of $n_o\varepsilon$ are chosen to examine the effects of the ring current at different stages of its development. Let ΔF_R denote the ring current field along an equatorial radius. The main part of the ring current field outside the ring is dipolar with the magnetic moment M_R. Thus the combined equatorial field intensity beyond the ring is given by

$$(M_E + M_R)/r_e^3 \, .$$

The flow of the solar plasma is affected by this combined dipole field. Thus, taking the radial distance of the front of the solar plasma to be r_B (in the equatorial plane), the field intensity ΔF_I due to the image dipole at a point r_e along the earth-sun line is given by

$$\Delta F_I = (M_E + M_R)/(2r_B \pm r_e)^3$$

(the plus sign refers to the night side and the minus sign to the day side). Therefore,

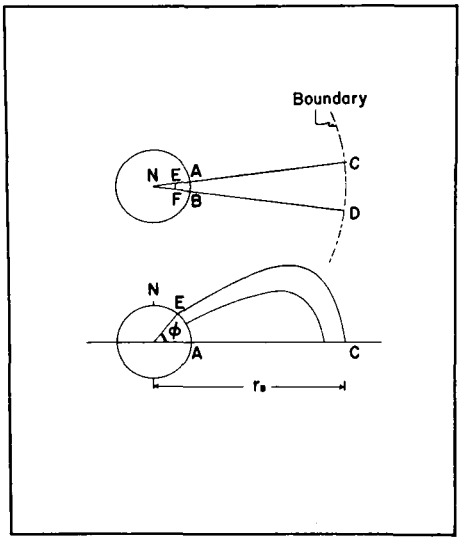

Fig. 17. The geometry for the calculation of the magnetic flux.

the total field intensity $F(r_e)$ along the earth-sun line, can be given, as a first approximation, by

$$F(r_e) = F_E + \Delta F_R + \Delta F_I ,$$

where we neglect the effects of the image dipole on the ring current (ΔF_I near the center line of the belt, $r_{eo} = 3a$, is less than 2% of the F_E field intensity for $r_B > 8a$).

In applying our calculations to the data obtained by a pair of satellites, like that of Injun I and Explorer XII, it is important to know, first of all, the location of two points on each distorted line of force, namely the point in the equatorial plane and that at the earth's surface, or actually the radial distance r_e of a point at which the line of force crosses the equatorial plane and the anchoring latitude ϕ (or the L value given by $1/\cos^2\phi$).

For this purpose, we use the magnetic flux conservation theorem, rather than tracing the distorted lines of force from the equatorial plane to the earth's surface. The

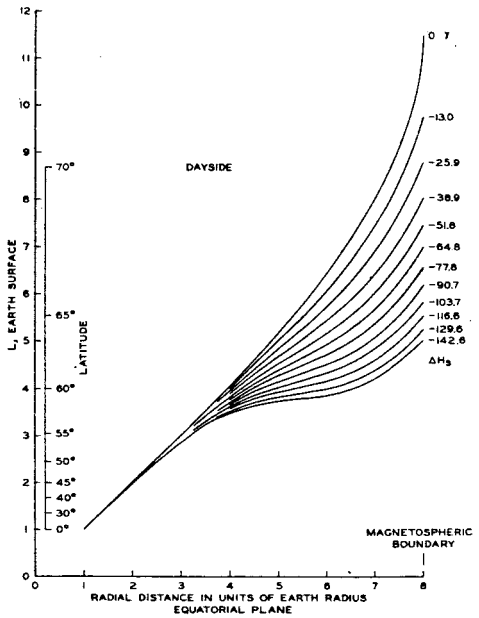

Fig. 18. (a) The r_e, L (or r_e, θ) relation for various intensity of the ring current. The magnetospheric boundary is taken to be $r_B = 8.0$ ($\Delta H_s = \Delta_1 F_s$).

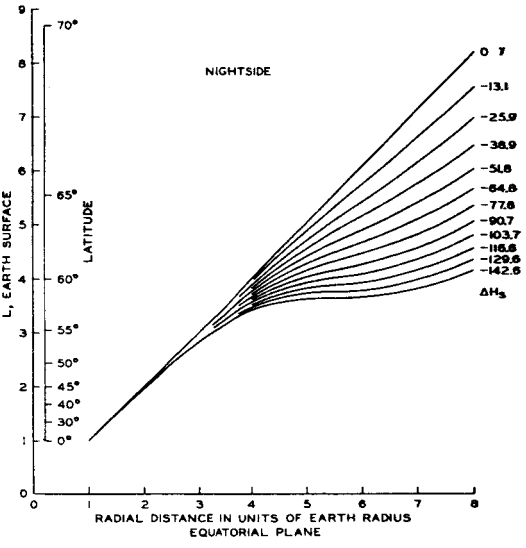

Fig. 18. (a) and (b), The r_e, θ (or r_e, L) relation in the noon and midnight meridian plane, respectively, for various intensity of the ring current. ($\Delta H_s = \Delta_1 F_s$).

flux G_e passing through the area $ABDC$, around the earth-sun line, in the equatorial plane (Figure 17), is given by

$$G_e = \int B \, dS = \int_a^{\lambda} \int B_e \, r_e \, dr_e \, d\lambda \, . \tag{48a}$$

This flux must be equal to the flux G_s coming into the earth's surface $ABEF$, namely

$$G_s = \int B \, dS' = \int_o^{\lambda} \int_o^{\phi} B_r a^2 \cos \phi \, d\phi \, d\lambda \, . \tag{48b}$$

In general, G_e is a function of r_e (in our example $r_e = r_B$), and G_s is a function of ϕ. For a dipole, the above two equations give

$$G_e = \int_a^{\lambda} d\lambda \int_a^{r_B} \left(\frac{B_0 a^3}{r_e^3} \right) r_e \, dr_e$$

$$G_s = \int_o^{\lambda} d\lambda \int_o^{\phi} 2B_0 \, a^2 \sin \phi \cos \phi \, d\phi \, ,$$

where B_0 (= 0.32 gauss) denotes the field intensity at the equator at the earth's surface. Equating the above two, we find simply the equation of the lines of force, namely

$$a = r_B \cos^2 \phi \, .$$

Our approach here for the distorted field F is to calculate first the total flux G_e in the equatorial plane and then to find the latitude ϕ, at which the integrated flux G_s from the equatorial plane becomes the same as G_e.

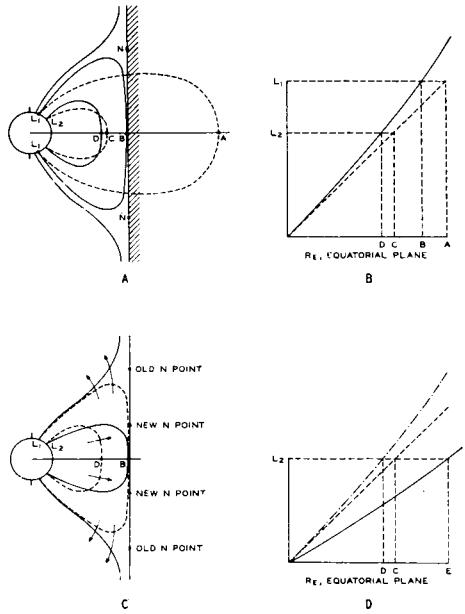

Fig. 19. The schematic diagram to show the interpretation involved in Figure 18.

Under the above scheme, the relation between r_e (the radial distance of the point at which the line of force crosses the equator) and the anchoring latitude ϕ (or $L = 1/\cos^2 \phi$) is obtained for various ΔF_s (the ring current field at the equator at the earth's surface). Hereafter, in this section, r_e and r_B are given in unit of the earth radius a; note that L is expressed in unit of a. The r_e, L (or r_e, ϕ) relation for $r_B = 8.0$ is given in Figures 18a and 18b.

For the earth's dipole field, the r_e, L relation in the Figure is expressed by a straight line, making an angle of $\pi/4$ with both the r_e and L axes, namely $r_e = L$. Any deviation from the straight line indicates a deviation of the line of force from the dipole line ($r = r_e \cos^2 \phi$). We show in a schematic way the implication of our r_e, L diagrams below and return to this point.

When a solar plasma advances towards the earth, two neutral points appear on the

plasma front, one on each side of the equatorial plane (CHAPMAN and FERRARO, 1931). In the noon meridian plane, the lines of force to these neutral points separate the lines of force that complete their course on the sunlit side of the earth, from those that close on the dark side. The further the advance of the plasma, the nearer are the neutral points to the equatorial plane; as they move towards this plane, some lines of force starting in high latitudes, which formerly lay on the day side, now are transferred to the night side. This action continues until the plasma front comes to a complete stop. Figure 19a shows this situation schematically when the front of the plasma (crudely treated as plane) is at geocentric distance $r_e = B$. The lines of force that originally crossed the equatorial plane at A are now "*compressed*" and lie just inside the plasma surface. The lines of force that originally crossed the equatorial plane at points beyond A are now transferred to the night side and close there. Such a change in the external field induces electric currents within the solid earth, which tend to prevent the penetration of external fields. Although the earth is not a perfect conductor, the induced currents hardly affect the latitudes at which the lines of force start from the earth. Because of the reduction of the radial distance from OA to OB, and because the anchoring L value (L_1 in Figure 19a) as shown in Figure 19b does not change appreciably, the original relation $r_e = L$ is altered, r_e now becomes less than L. Similarly, the line of force through C moves to D, but again the anchoring point is unchanged (L_2).

Suppose now that the plasma is stopped at B ($r_e = B$) and that the ring current begins to grow in the area enclosed by the deformed line of force $r_e = D$ (Figure 19c). As seen in Section 5 (Figure 9), the growth of the ring current tends to stretch the lines of force that pass between the ring and the plasma front. At a certain epoch of the main phase, the line through D in Figure 19a has moved outward to a point just inside the boundary surface $r_e = B$. The lines of force which crossed the equatorial plane between $r_e = D$ and $r_e = B$ in Figure 19a are stretched and then transferred to the night side. Note that if the boundary position B is fixed while the ring current is growing, there must be an increase of the plasma pressure in order to balance the growth of the ring current pressure; there is some evidence to support this; about or a little after the maximum epoch of the main phase of the magnetic storms of September 30, and October 28, the magnetospheric boundary on the dayside was closer to the earth than its average position (FREEMAN, VAN ALLEN and AKASOFU, to be published). Because $r_e = D$ has moved to $r_e = B$ and because the point L_2 does not change appreciably, the curve in Figure 19b is flattened as is seen in Figure 19d. The image dipole and the ring current have opposed effects.

Figure 18 consists of two parts, one for the day side and one for the night side. The considerable difference between them corresponds to the fact that the image dipole field is more intense on the dayside than on the night side. However, the image dipole approximation is less accurate on the night side. To find the corresponding lines of force which constitute a magnetic L surface, it is necessary to calculate the second integral invariant I along the lines of force.

In Figure 18, the deviation from the straight line becomes serious beyond $r_e = 3.0$

even for a medium storm. Beyond $r_e = 4.0$, the deformation is considerable even for a weak ring current.

We have seen earlier that there is a quiet-time proton belt, and it has been shown that it can produce a field $\Delta_1 F_s$ of order -40γ. Any Dst change of the horizontal component of the earth's field must be regarded as superposed on the field of this proton belt; this point will be discussed further in later sections.

The induction effect discussed in Section 1 must be taken into account to relate the observed Dst(H') change to the true Dst(H), namely Dst(H') = 1.5 Dst(H). Figure 24b has three scales, of abscissae, for $\Delta_1 F_s$, Dst(H) and Dst(H').

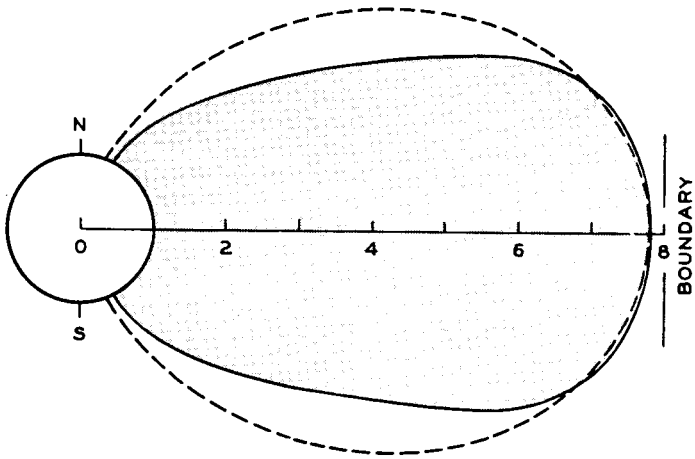

Fig. 20. The distorted line of force of $r_e = 7.8$ in the noon meridian, together with the dipole field line crossing the equator at the same point. The magnetospheric boundary is at 8.0 and the intensity of the ring current is Dst(H') $\simeq -150\ \gamma$. The area enclosed by the distorted field line is shaded to show approximately the cross-section of the outer belt during the main phase of magnetic storms.

The explorer XII satellite showed that the outer boundary of the outer radiation belt coincides with the magnetospheric boundary on the day side, where the solar plasma acts on the magnetic field (FREEMAN, VAN ALLEN and CAHILL, 1963). Figure 19a shows that for Dst(H) $\simeq -150\gamma$, the line of force that originally crossed the equatorial plane at $r_e = 5.0$ is now stretched out to $r_e = 8.0$. To examine this point more clearly, the line of force anchored at $L = 4.8 (\phi = 62.5°)$ is calculated under the same condition, and is shown in Figure 20. Note that it is stretched out to $r_e = 7.8$, so that in terms of the parameter L, two satellites, like Injun I and Explorer XII (see Figure 16a), will see the difference of 7.8 − 4.8 = 3.0. We infer that such a reduction corresponds to the low L value observed by Injun I during the October 28, 1961 storm. Further, we may take this agreement to be important evidence that the storm-time ring current is embedded within the outer radiation belt.

It is known that the center line of the auroral zone approximately agrees with the

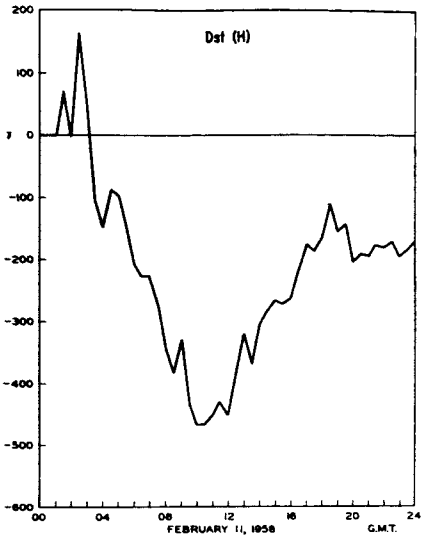

Fig. 21. The Dst(H') curve for the storm of February 11, 1958, obtained from 8 low-latitude observatories.

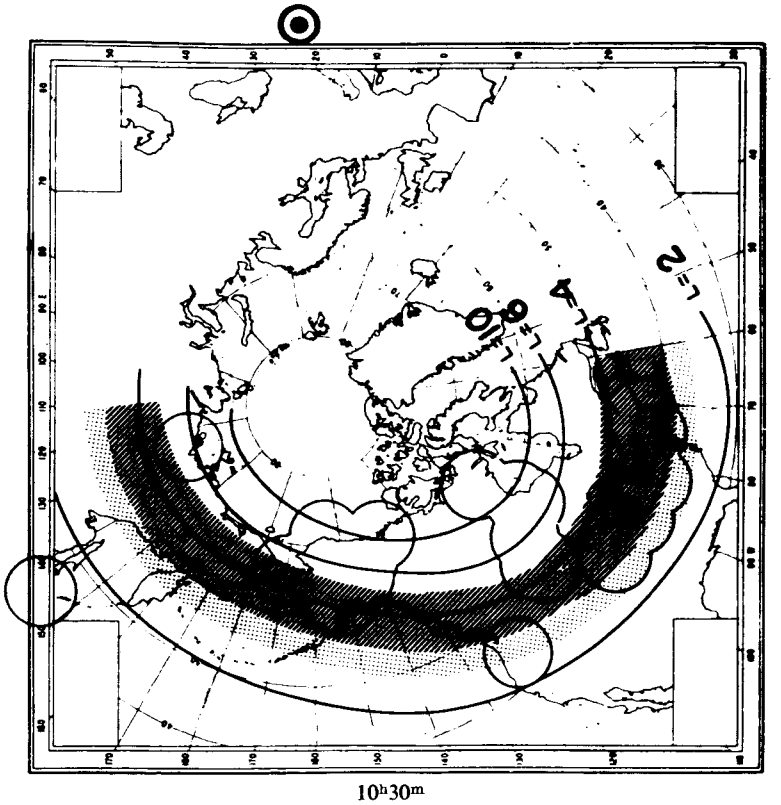

10^h30^m

Fig. 22. The distribution of the auroras at 1030 GMT, February 11, 1958 from 23 all-sky camera stations.

$L = 6.0$ line at the earth's surface, but the above discussion shows that during magnetic storms the lines of force anchored in the auroral zone do not, in general, cross the equatorial plane at the radial distance $r_e \sim 6.0$. During a large main phase, r_e could exceed 10 on the night side.

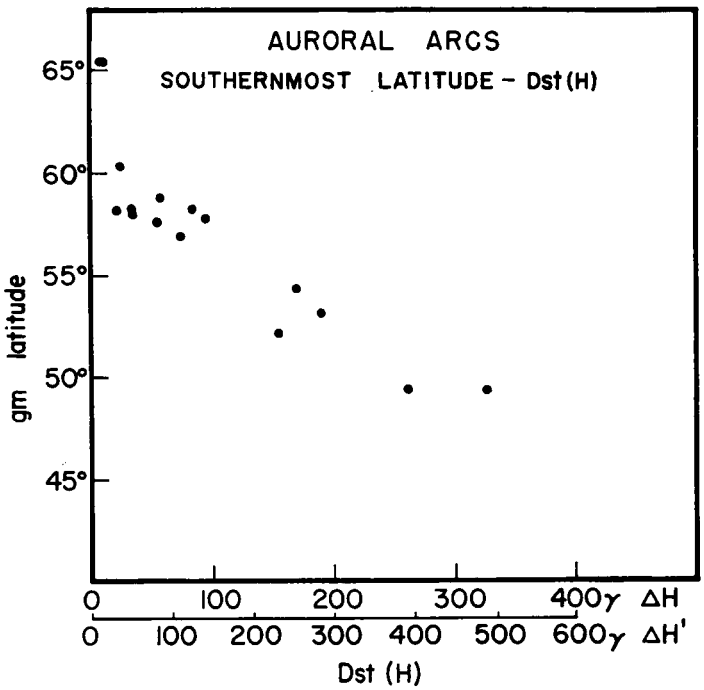

Fig. 23. The relation between the lower limit of latitude attained by quiet arcs in the US sector during 16 magnetic storms, and the intensity of the magnetic field produced by the ring current. ($\Delta H = \mathrm{Dst}(H)$, $\Delta H' = \mathrm{Dst}(H')$).

B. LATITUDE DECREASE OF POLAR AURORAS DURING LARGE MAGNETIC STORMS

The lowering of the boundary L value of the outer radiation belt near the earth seems to be closely related to the equatorward shift of the regions in which overhead auroras are seen, and to other related geophysical phenomena during magnetic storms.

A spectacular equatorward shift of the auroral strip occurred during the great magnetic storm of February 11, 1958, which had an exceptionally large Dst decrease exceeding 450γ (Figure 21). At about 1020 GMT on February 11, around the maximum epoch of the Dst decrease, the auroral zone in the North American Continent and in a part of Siberia was completely deserted; but while there was no indication of bright auroral arcs along the auroral zone, there were active auroras far to the south, (Figure 22).

Figure 23 summarizes the relation between the Dst decrease and the lower limit of

latitude attained by quiet arcs in the US sector (based on 16 magnetic storms during the IGY). The equatorward shift of quiet arcs is clearly related to the growth of the ring current.

C. ANOMALOUS ENTRY OF NON-RELATIVISTIC SOLAR PROTONS

The modification of the Störmerian orbits of non-relativistic solar protons by the ring current field does not explain their observed penetration into the magnetosphere (Section 7). This is because the magnetic moment M_R of the ring current does not

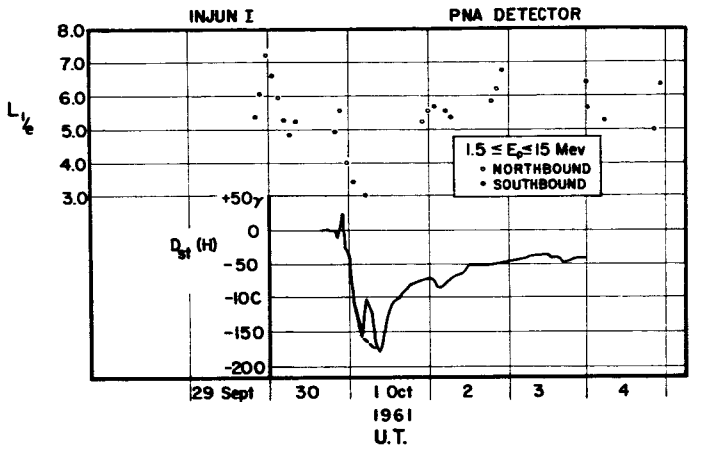

Fig. 24a. The relation between the lowest L value attained by solar protons (of energy between 1.5 and 15 MeV) and the Dst(H') during the September 30 magnetic storm. (VAN ALLEN, 1962).

seem to exceed that of the earth; to explain some of the solar proton observations, however, M_R/M_E would have to be larger than 10, which seems not possible.

Nevertheless, the anomalous entry of the protons seems to occur during storms with a considerable main phase; Figure 24a shows such an example during September 30–October 1, 1961. The difficulty may perhaps be overcome by taking account of the limited extent of the magnetosphere, including the ring current field. Explorer XII observations indicate that the earth's magnetic field is present only within a cavity in the stream of solar plasma.

If the boundary is at $8a$ to about $10a$, solar protons of very low energy can reach the surface of the magnetosphere in the equatorial plane without any difficulty, particularly when the boundary is within $10a$ (in the equatorial plane), a distance that non-relativistic solar protons of order 10 Mev or less cannot attain in an unmodified dipole field.

AKASOFU, LIN and VAN ALLEN (1963) have shown that there is always an allowed region within a boundary that extends from the equatorial plane to the polar cap, and lies very closely along the lines of force that cross the equator just inside the boundary.

We have already seen in Section 8A that during the main phase of a magnetic storm the lines of force anchored at $L = 5.0$ can be stretched to the boundary ($r_e \sim 8.0$). Therefore, in such a situation, solar protons of energy as low as 500 kev can reach the point $L = 5.0$ ($\phi = 63.5°$) after penetrating the magnetospheric boundary in the equatorial plane. Figure 24b shows the relation between such L or ϕ and the equatorial intensity of the ring current field at the earth's surface. If Dst(H) is superposed on a constant $\Delta_1 F_s$, even the quiet-time proton belt contributes considerably to the anoma-

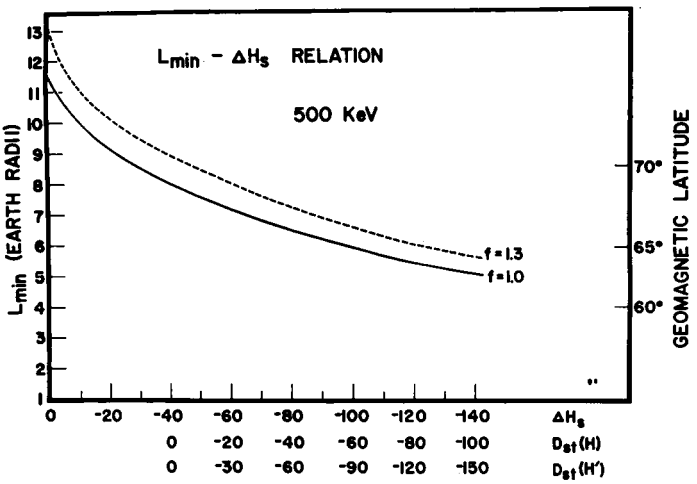

Fig. 24b. The relation between the minimum L value attained by solar protons of energy 500 kev and the intensity of the ring current.

lous entry; note that for the earth's dipole field, STÖRMER's cut-off latitude is 78° and that even a large storm-time ring current cannot produce this reduction if both the earth's field and the ring current field extend to infinity.

D. EXPANSION OF THE OUTER RADIATION BELT

Another significant observation made by Explorer XII was a remarkable expansion of the outer radiation belt during the recovery phase of certain magnetic storms. This may be explained as a combined effect of a decrease of the solar plasma pressure and an increased ring current pressure. The ring current strengthens the earth's field outside the ring current belt.

Let m, n and V denote respectively the mass, number, density, and speed of the solar plasma. Where the plasma boundary cuts the earth-sun line, the plasma pressure $p = 2mnV^2$ is balanced by the magnetic pressure $B_B^2/8\pi$ (here B_B denotes the boundary intensity of the magnetic field

$$\frac{B_B^2}{8\pi} = 2mnV^2 .$$

We take, as an example, $n = 1.0/\text{cm}^3$ and $V = 10^8$ cm/sec. For this particular case, the boundary will appear at a point where the field intensity at the boundary B_B becomes 91.2γ. The boundary is then located at a point where the earth's field intensity is $B_B/2 = 45.6\gamma$, namely $r_B = 8.9a$. If the ring current is present, the boundary for the above plasma pressure is now located at a point where the combined field intensity $F = F_E + \Delta F_R$ is 45.6 γ (cf. SPREITER and ALKSNE, 1962).

Assuming the model ring current given by the parameters $r_{eo} = 3.0a$, $g_1 = 2.990$,

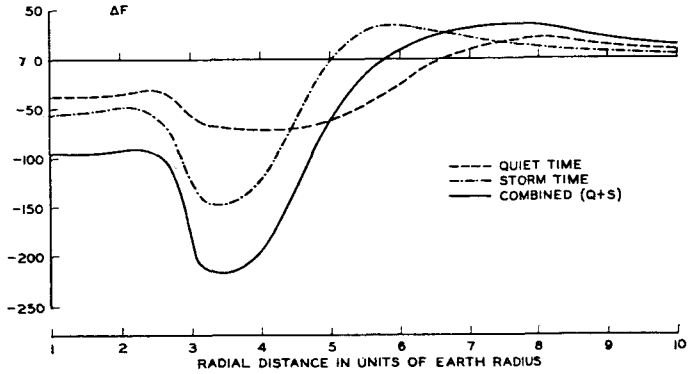

Fig. 25. The distribution of the magnetic fields $\Delta_1 F$ for the quiet-time proton belt, for the storm-time belt and the combined belt.

$g_2 = 0.419$ and $\alpha = 2.0$, with $\text{Dst}(H) \simeq -50\gamma$, the boundary will appear at $r_B = 9.8a$ for the same plasma pressure. If this pressure decreases to half the value, the boundary will move to $r_B = 11.1a$, an expansion of $2.2a$; this is about what Explorer XII observed. This is another indication that there is a storm-time ring current belt within the outer radiation belt.

9. The Storm-Time Ring Current

A. SATELLITE OBSERVATIONS

Calculations show that a distribution of trapped particles around the earth will produce a magnetic field that is nearly uniform and parallel to the dipole axis within 2 or 3 earth radii. This calculated field agrees with what the Dst analysis indicates. Other important features of the radiation belt regions during the main phase can also be explained by assuming the growth of a ring current belt embedded in the outer radiation belt.

Satellite observations have shown that there is a quiet-time proton belt, which distorts the earth's magnetic field appreciably by its ring current.

So far, however, we have not obtained any definite satellite information concerning the belts that are responsible for the storm-time ring current. Because the quiet-time

proton belt itself is capable of producing $\Delta_1 F_s \simeq -40\gamma$ (at the equator at the earth's surface), storm-time changes of the belt may be expected to contribute significantly to the Dst change. DAVIS and WILLIAMSON (1962) infer from their Explorer XII data that during the recovery phase of the September 30, 1962 storm the proton belt flux was probably enhanced about threefold at the center line of the belt, $r_{eo} = 3.2a$. AKASOFU and CAIN (1962) showed that such an enhancement is enough to produce the observed Dst decrease (Figure 25). This enhancement occurred in the energy range of 150 kev–4.5 Mev. The other radiation belts, such as the "classical" electron outer belt, the low energy outer belt and the inner belt, cannot produce any significant distortion of the earth's field.

A proper understanding of the changes in the ring current belt during magnetic storms can be gained only by continued satellite observations. Their results must be studied alongside the simultaneous magnetic records at magnetic observations.

So far, we know that the main phase occurs not only at the earth's surface, but also in a region beyond the ionosphere (CAIN, SHAPIRO, STOLARIK and HEPPNER, 1962; SMITH and SONETT, 1962; CAHILL, 1962). This agrees with earlier conjectures that the major part of the Dst decrease is produced by a source located in a region at least a few earth radii away from the earth.

B. ENERGY INPUT

The growth of the ring current belt within the magnetospheric region is undoubtedly caused by solar action. However, we do not yet know the energy spectrum of the solar plasma, nor how the plasma generates the ring current belt within the magnetosphere.

The total number of particles in a model belt of the type discussed earlier is as follows:

$$N = \int n \, \mathrm{d}V$$

$$= \int\int\int n(r_e, \phi)\, r^2 \cos^7 \phi \, \mathrm{d}r_e \, \mathrm{d}\phi \, \mathrm{d}\lambda \, .$$

Introducing Equations (29), (30) and (33), this may be rewritten as

$$N = \frac{2\pi I_F}{B(\alpha)} \int_{-\infty}^{\infty} n(r_e) r_e^2 \, \mathrm{d}r_e$$

$$= \frac{2\pi I_F n_o a^3}{B(\alpha)} \left[\frac{\sqrt{\pi} f_o^2}{2} \left(\frac{1}{g_1} + \frac{1}{g_2} \right) + \frac{\sqrt{\pi}}{4} \left(\frac{1}{g_1^3} + \frac{1}{g_2^3} \right) + f_0 \left(\frac{1}{g_1^2} - \frac{1}{g_2^2} \right) \right]$$

where

$$I_F = \int_0^{\pi/2} \frac{2B(\alpha)(\cos\phi)^{3\alpha+7}}{(1 + 3\sin^2\phi)^{\frac{1}{2}\alpha}} \mathrm{d}\phi$$

This function I_F is tabulated in a paper by AKASOFU and CHAPMAN (1961); for $\alpha = 2.0$

$$I_F = 0.1262 \, .$$

TABLE

MODEL BELT *

$r_{eo}(a)$	2.0	3.0	4.0	5.0	6.0
Maximum $\Delta_1 F_s$ (γ)	− 270	− 155	− 100	− 55	− 30
Maximum Dst(H′) (γ)	− 405	− 233	− 150	− 83	− 45
Maximum $n_o\varepsilon$ (Kev/cm³)	3500	1200	500	200	85
N/n_o	4.59^{27}	1.16^{28}	2.26^{28}	3.89^{28}	6.03^{28}
Total particle energy $N\varepsilon$ (ergs)	2.58^{22}	2.23^{22}	1.81^{22}	1.25^{22}	7.47^{21}

* $g_1 = 2.990, g_2 = 0.419, \alpha = 2.0$.

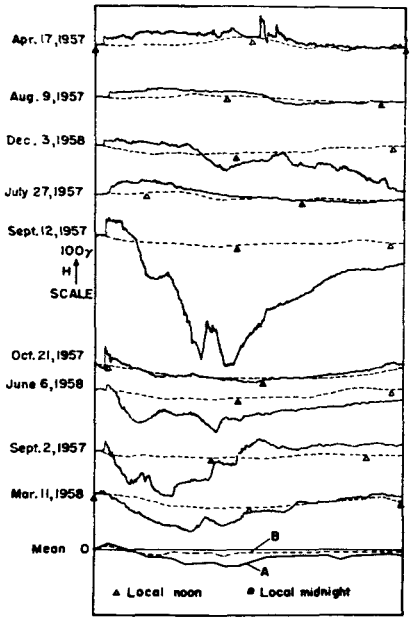

Fig. 26. The horizontal component magnetograms from the Honolulu station showing the variety of the development of the main phase.

For a belt of the type discussed in Section 7 (namely, $g_1 = 2.990, g_2 = 0.419, \alpha = 2.0$), the table above gives, for different values of the center line of the belt r_{eo}, approximate values of (i) the maximum field $\Delta_1 F_s$ produced at the equator at the earth's surface: (ii) the Dst(H') $\simeq 1.5 \times \Delta_1 F_s$, (iii) the maximum particle energy density $n_o\varepsilon$ at r_{eo}, (iv) N/n_o, and (vi) the total particle energy $N\varepsilon$ ($= n_o\varepsilon \times N/n_o$). For this model belt, the total particle energy required for the largest Dst decrease (-405γ) is 2.58×10^{22} ergs.

Further, if the center line of the belt is located at $r_{eo} = 3a$, for a medium storm of $\mathrm{Dst}(H') \simeq -100\gamma$, $N\varepsilon = 10^{22}$ ergs. This is similar in order of magnitude to the change in the magnetic field energy (CHAPMAN and BARTELS, 1940, p. 897).

It has been pointed out by PARKER (1962) that this amount of particle energy is equivalent to the accumulation of kinetic energy flux of the solar plasma ($v = 1500$ km/sec, $n = 50$ protons/cm^3, over a cross section with 4 earth radii radius) in less than 10 seconds. Thus the solar plasma that causes the sudden commencement and the

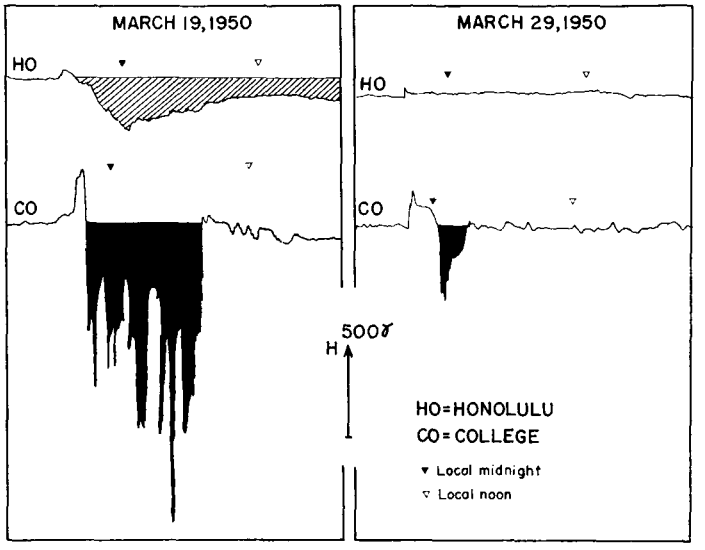

Fig. 27. The horizontal component magnetograms of a highly contrasted pair of storms from the Honolulu and College stations.

initial positive phase seems to have ample energy to produce the ring current and the main phase.

However, this does not solve the problem of the formation of the enhanced ring current belt, nor do we know why the solar plasma, on different occasions, gives different types of development of the main phase. Figure 26 shows the H variations during several magnetic storms at Honolulu, a typical low latitude station (geomagnetic latitude 21° N). For comparison, each dotted curve shows a quiet day H variation recorded during the month of each storm. The first storm, of April 17, 1957, showed a remarkable *ssc* and a long initial phase of more than eight hours, with no significant main phase. The last storm, of March 11, 1958, is at the other extreme; it showed a very small *ssc* and a short initial phase, but a fairly large main phase, which started soon after the *ssc*. The July 11 and 15, 1959 storms in Figures 1 and 2 also show such a highly contrasted pair.

The occurrence of storms like those of April 17, 1957 and July 11, 1959, with a large and long initial phase, but with no appreciable main phase, indicates that a solar plasma producing the *ssc* or the initial phase does not necessarily enhance the ring current. What we observe in the magnetic records is the combination of the positive solar effect of the plasma and the negative effect of the ring current. One might therefore argue that in such cases, the ring current effect was overcome by the positive effect. It seems, however, that except during very intense storms, the positive effect is not more than 70γ, and for the above two cases, perhaps of order 10γ to about 30γ. Explorer XII data showed that the minimum geocentric distance of the plasma boundary during its life time was of order $r_B = 8a$. Magnetic records from high latitude regions are more varied in this respect. In Figure 27, the main phase decrease is hatched in the Honolulu magnetograms, and the polar magnetic sub-storms shown by those for College are shaded. Notice the great differences in the development of both the main phase and polar magnetic storms. Particularly, the storm of March 29, 1950 did not seem to have any appreciable main phase; polar storms at College are almost daily events, and can occur without any definite sign of *ssc*. When the development of the main phase is intense, the auroral activity is also considerable (because the development of polar magnetic storms is closely related to the auroral activity).

C. TWO-BELT MODEL

Figure 28 shows the H variations during several magnetic storms at Honolulu. Clearly there is a systematic difference in the growth and decay of the main phase, depending on the intensity. This may reasonably be interpreted by supposing that the main phase is composed of two parts, most clearly characterized by their decay rates. One decays much more rapidly than the other; thus they may be denoted by F and S, respectively; F refers to the fast decay and S the slow decay: their relations are schematically shown in Figure 29.

The parts F (DR1) and S (DR2) differ systematically in their intensities, depending on the magnitude of the Dst decrease. They are larger for more intense magnetic storms. Further, the development of the part F is much more remarkable in greater storms, particularly in many of the historic greatest storms. For such greatest storms, F decays so rapidly that the combination of the parts F and S shows a rather sharp change of the decay rate. This apparent discontinuity in the decay rate has been examined for many other storms. In weaker storms of the Dst(H') $\simeq -100\gamma$, the development of the part F seems to be less than that of the S. In still weaker storms, it may hardly be recognized.

On the other hand, the development of the part S seems less dependent on the magnitude of magnetic storms. Extraordinarily intense storms, such as the September 13, 1957 and the February 11, 1958 storms, are largely due to an abnormal growth of the part F.

A reasonable way of interpreting this phenomenon, based on the Table, is to assume that there are two ring current belts, at different places. Because the part F can contribute as much as 300γ or more to Dst(H), and because it decays much more

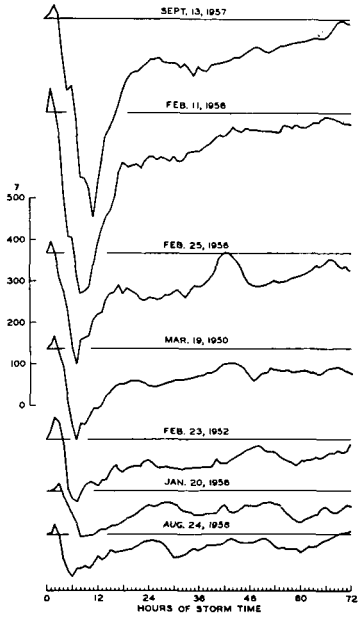

Fig. 28. The horizontal component changes at the Honolulu station showing a systematic difference in the extent of growth and the mode of decay of the main phase, depending on the magnitude of the main phase decrease.

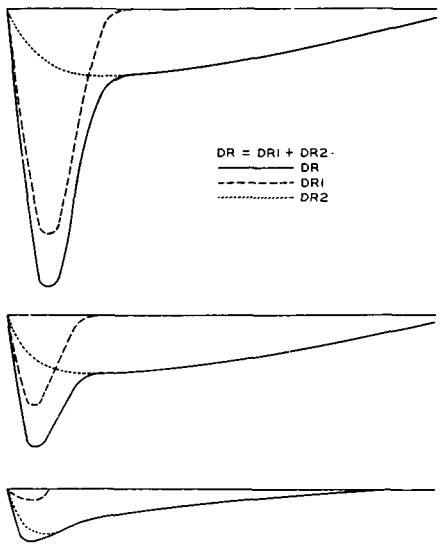

Fig. 29. The schematic diagram to show that the main phase decrease is composed of two parts, DR1 and DR2.

rapidly, the belt that produces the F is probably closer to the earth than is the S belt. Possibly they consist of particles of different energies, or differ both in location and energy.

Particularly for the belt that is responsible for the F, there are two competing effects, namely the energy input mechanism and the energy dissipation mechanism. During the growth stage, the input energy must exceed the dissipation. At the maximum epoch of the main phase, the two mechanisms balance each other. Thus the input energy must begin to decrease a little earlier than the time of maximum Dst(H). This suggests also that it is not right to calculate the rate of input energy by simply dividing the total energy in the Table by the time interval between the beginning of the main phase and its maximum epoch. There are many complicated storms which could be intermediate cases between any two of the storms in Figure 28. (See also Figure 30).

The direct injection of energetic solar particles has long been thought to be the source of the ring current particles. In order to have Dst(H') of order -150γ at the earth's surface, however, the center line of the belt should be $r_{eo} \simeq 4a$ or less. Direct penetration to such a depth from outside the magnetospheric boundary could be attained by some of non-relativistic solar cosmic rays, but their flux is much too low to form an appreciable ring current.

Assuming that 30 Mev protons can penetrate down to $r_{eo} = 4.0a$ in the equatorial

plane (although such a deep *direct* penetration does not seem to occur), the number density n_o required for $\mathrm{Dst}(H') \simeq -150\gamma$ is $500(\mathrm{kevcm^3})/3 \times 10^4(\mathrm{kev}) = 0.017/\mathrm{cm^3}$; the flux is then $n_o w = 0.017\ (\mathrm{cm^3}) \times 7.58 \times 10^9\ (\mathrm{cm/sec}) = 1.36 \times 10^8/\mathrm{cm^2}$ sec. Satellite observations indicate that the flux of 30 Mev solar protons outside the magnetosphere is of order $10^3/\mathrm{cm^2}$ sec at most. This is negligible compared with the

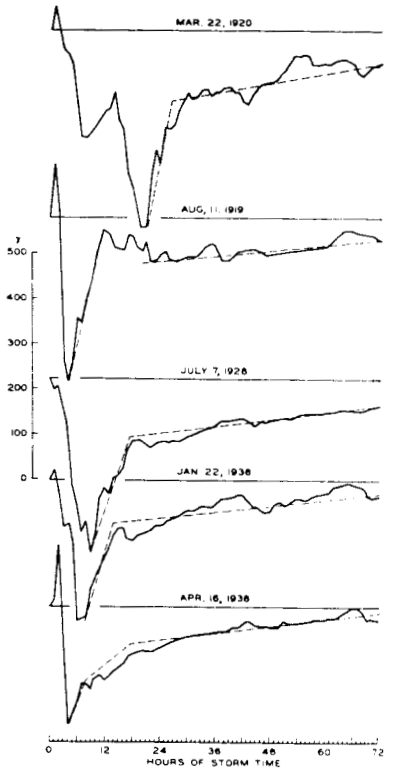

Fig. 30. The horizontal component changes at the Honolulu station for some of the most severe magnetic storms in the past.

required number. The flux of non-relativistic solar protons increases rapidly towards lower energies, but it does not seem possible for 1 Mev protons to penetrate as close as $r_e \approx 4a$ or less. Satellites do not show any sign of the formation of the belt by these protons. This difficulty was pointed out by DESSLER, HANSON and PARKER (1961). Instead of direct injection, they proposed that hydromagnetic heating can raise the energy of thermal protons in the magnetosphere to a few kev. They infer that wherever the solar plasma comes in contact with the geomagnetic field, hydromagnetic waves are generated at the interacting surface. They infer also that the ratio $\Delta B/B$ of the amplitude of the waves to the dipole field intensity would be of order unity at about $r_e = 3a \sim 5a$ (see also PARKER, 1962; pp. 89–91): the waves generated at the interacting

boundary develop into shock waves with a sharp crest, resulting in a rapid dissipation of the wave energy, presumably by instabilities of anisotropic thermal motions of particles and others. Recently, KERN (1962) elaborated further this problem.

However, it is uncertain whether ΔB (of period 30 seconds or less) can be as large as $250\gamma \sim 1000\gamma$ at $r_e = 3a$ to about $5a$. So far, satellites have not encountered any such violent magnetic fluctuations. Further, if the earth's field is so much disturbed, as they suggest, it would hardly be possible to have any systematic ring current to produce the main phase. The difficulty would be increased further for a large Dst change of more than 300γ. The formation of the ring current belt which produces such a considerable change would require ΔB to be as large as 4000γ at $r_e = 2a$. Furthermore, as we saw in Figures 26 and 27, the contact of the solar plasma at the interacting surface does not necessarily lead to the formation of the ring current. It seems that their proposed mechanism in its present stage involves as many difficulties as the direct injection.

The variety of development of storms shown in Figures 26 and 27 suggests intrinsic differences between the solar streams, far beyond what we would expect from a mere difference between their pressures. The nature of these intrinsic differences is at present unknown. A simple model would be to assume an energy source, whatever it may be, for the main phase and for the auroral activity, distributed differently for different solar streams. The existence of storms with a large and long initial phase, but with no appreciable main phase, suggests that some of the solar plasma would not include any appreciable amount of such energy, at least along the sun-earth line. The variety of development seen in Figures 26 and 27 would then be interpreted in terms of differences between the distribution and the intensity of such an energy source in the solar plasma. Satellite observations of various physical quantities in the interplanetary space, as well as in the magnetosphere, are extremely important from this view point.

Appendix
The Dst Analysis

Let H' denote the instantaneous values of the horizontal component of the geomagnetic field at station j. The deviation of the above values from a certain time $t = 0$ may be denoted by $\Delta H'$. The average storm-time variations $\mathrm{Dst}(H')$ is then defined by

$$\mathrm{Dst}(H') = \sum_{j=0}^{J} \frac{\Delta H'(t, \phi)}{J},$$

where J denotes the number of stations distributed along a circle of geomagnetic latitude ϕ.

Here the base value for H' may be taken to be the value just before the sudden commencement of magnetic storms, and t may be reckoned from the time of sudden commencement. Usually, the stations are chosen within the belts between $+5°$ and

25° gm. latitudes and between −5° and −25°. If the number of the stations is more than 8 and if they are well distributed in longitude, the effect of the Sq variation would be eliminated. (Because of a large Sq variation, it would not appropriate to choose stations located close to the magnetic equator.) If it is desirable to eliminate the Sq variation, we find a typical Sq curve of the month of the storm for each station and then adjust the base value of the Sq variation, so that at $t = 0 (= t' =$ local time) the storm curve and the Sq curve cross each other. Thus,

$$\Delta H' = H' - \mathrm{Sq}(H')$$

where $\mathrm{Sq}(H')$ denotes the adjusted Sq, so that at $t = 0$, $H' - \mathrm{Sq}(H') = 0 (= \Delta H')$.

Acknowledgements

I wish to express my sincere thanks to Dr. S. CHAPMAN and Dr. J. C. CAIN for many helpful suggestions and discussions. I am also greatly indebted to Dr. J. A. VAN ALLEN and his associates for their valuable discussions. The research reported here was supported by a grant from the National Aeronautics and Space Administration (NsG 201–62).

References

Section 1.

ALFVÉN, H.: 1958, 'On the theory of magnetic storms and aurorae', *Tellus* **10**, 104–116.

CHAPMAN, S.: 1919, 'An outline of a theory of magnetic storms', *Proc. Roy. Soc. London, A*, **95**, 61–83.

CHAPMAN, S. and FERRARO, V. C. A.: 1933, 'A new theory of magnetic storms', *Terr. Magn.* **38**, 79–96.

CHAPMAN, S.: 1935, 'The electric current-systems of magnetic storms', *Terr. Magn.* **40**, 349–370.

CHAPMAN, S.: 1951, 'The earth's magnetism, Methuen's monograph on physical subjects.

CHAPMAN, S. and BARTELS, J.: 1940, *Geomagnetism*, Oxford Press.

SINGER, S. F.: 1957, 'A new model of magnetic storms and aurorae', *Trans. Amer. Geophys. Union* **38**, 175–190.

SUGIURA, M. and CHAPMAN, S.: 1960, 'The average morphology of geomagnetic storms with sudden commencement', *Abhandl. Akad. Wiss. Göttingen, Math.-Phys. Kl.*

Section 2.

ALFVÉN, H.: 1950, *Cosmical electrodynamics*, Oxford University Press.

KULSRUD, R. M.: 1957, 'Adiabatic invariant of the harmonic oscillator', *Phys. Rev.* **106**, 205–207.

MCILWAIN, C.: 1961, 'Coordinates for mapping the distribution of magnetically trapped particles', *J. Geophys. Res.* **66**, 3681–3691.

NORTHROP, T. G. and TELLER, E.: 1960, 'Stability of the adiabatic motion of charged particles in the earth's field', *Phys. Rev.* **117**, 215–225.

STÖRMER, C.: 1955, *The polar aurora*, Oxford University Press.

VAN ALLEN, J. A.: 1962, 'Dynamics, composition and origin of the geomagnetically-trapped corpuscular radiation', *Trans. Int. Astron. Union* **11B**.

Section 3.

COLEMAN, P. J., Jr.: 1961, 'The effects of betatron accelerations upon the intensity and energy spectrum of magnetically trapped particles', *J. Geophys. Res.* **66**, 1351–1361.

PARKER, E. N.: 1957, 'Newtonian development of the hydromagnetic properties of ionized gases of low density', *Phys. Rev.* **107**, 924–933.

SPITZER, L., Jr.: 1952, Equations of motion for an ideal plasma, *Astrophys. J.* **116**, 299–316.

Section 4.

AKASOFU, S.-I.: 1962, 'On a self-consistent calculation of the ring current field', *J. Geophys. Res.* **67,** 3617–3618.

BEARD, D. B.: 1962, 'Self-consistent calculation of the ring current', *J. Geophys. Res.* **67,** 3615–3616.

LINHART, J. G.: 1960, *Plasma Physics,* North-Holland Publ. Comp., Amsterdam.

Section 5.

AKASOFU, S.-I., CAIN, J. C., and CHAPMAN, S.: 1961, 'The magnetic field of a model radiation belt, numerically computed', *J. Geophys. Res.* **66,** 4013–4026.

AKASOFU, S.-I., CAIN, J. C., and CHAPMAN, S.: 1962, 'The magnetic field of the quiet-time proton belt', *J. Geophys. Res.* **67,** 2645–2647.

AKASOFU, S.-I. and CHAPMAN, S.: 1961, 'The ring current, geomagnetic disturbance, and the Van Allen belts', *J. Geophys. Res.* **66,** 1321–1350.

APEL, J. R., SINGER, S. F., and WENTWORTH, R. C.: 'Effects of trapped particles on the geomagnetic field', Tech. Rep. No. 237, Physics Dept., University of Maryland.

APEL, J. R., SINGER, S. F., and WENTWORTH, R. C.: 1961, 'Effects of trapped particles on the geomagnetic field', Tech. Rep. No. 237, Physics Dept., University of Maryland.

DAVIS, L. R. and WILLIAMSON, J. M.: 1962, 'Low energy trapped protons', paper presented at the third International Space Science Symposium, April 30–May 9.

DESSLER, A. J. and PARKER, E. N.: 1959, 'Hydromagnetic theory of geomagnetic storms', *J. Geophys. Res.* **64,** 2239–2259.

Section 6.

AKASOFU, S.-I., CAIN, J. C., and CHAPMAN, S.: 1961 in Section 5.

Section 7 and 8.

AKASOFU, S.-I. and CAIN, J. C.: 1962, 'The magnetic field of the radiation belts', *J. Geophys. Res.* **67,** 4078–4080.

AKASOFU, S.-I. and CHAPMAN, S.: 1962, 'Large-scale auroral motions and polar magnetic disturbances', *J. Atmosph. Terr. Phys.,* **24,** 785–796.

AKASOFU, S.-I. and CHAPMAN, S.: 1963, 'The lower limit of latitude (U.S. sector) of northern quiet auroral arcs, and its relation to Dst(H)', *J. Atmosph. Terr. Phys.* **25,** 9–12.

AKASOFU, S.-I., LIN, W. C., and VAN ALLEN, J. A.: 'The anomalous entry of non-relativistic solar protons into the geomagnetic field', *J. Geophys. Res.* **68.**

AKASOFU, S.-I. and LIN, W. C.: 1963, 'The magnetic moment of model ring current and the cut-off rigidity of solar protons', *J. Geophys. Res.* **68,** 973–977.

AKASOFU, S.-I., VAN ALLEN, J. A., and FREEMAN, J. W.: 1963, 'Deformation of the magnetic shells during magnetic storms', *J. Geophys. Res.* **68** (August issue).

CHAPMAN, S. and FERRARO, V. C. A.: 1931, 'A new theory of magnetic storms', *Terr. Magn.* **36,** 77–97.

FREEMAN, J. W., VAN ALLEN, J. A., and CAHILL, L. J.: 1963, 'Particle and magnetic observations of the magnetospheric boundary and solar plasma with Explorer XII', *J. Geophys. Res.* **68,** 2121–2130.

KELLOGG, J. P. and WINCKLER, J. R.: 1961, 'Cosmic ray evidence for a ring current', *J. Geophys. Res.* **66,** 3991–4001.

MAEHLUM, B. and O'BRIEN, B. J.: 1963, 'Study of energetic electrons and their relationship to auroral absorption of radio waves', *J. Geophys. Res.* **68,** 997–1010.

MCILWAIN, C.: 1961, in Section 2.

SPRITER, J. R. and ALKSNE, A. Y.: 1962, 'On the effect of a ring current on the terminal shape of the geomagnetic field', *J. Geophys. Res.* **67,** 2193–2205.

Section 9.

AKASOFU, S.-I. and CAIN, J. C.: 1962, 'A model storm-time proton belt', *J. Geophys. Res.* **67,** 3537.

AKASOFU, S.-I. and CHAPMAN, S.: 1961 in Section 5.

AKASOFU, S.-I. and CHAPMAN, S.: 1963, 'The development of the main phase of magnetic storms', *J. Geophys. Res.* **68,** 125–129.

AKASOFU, S.-I., CHAPMAN, S., and VENKATESAN, D.: 1963, 'The main phase of great storms', *J. Geophys. Res.* **68,** 3345–3350.

CAHILL, L. J., Jr. and AMAZEEN, P. G.: 1962, 'Termination of the earth's magnetic field during the period September 11–14, 1961', *J. Geophys. Res.* **67,** 3547.

CAIN, J. C., SHAPIRO, I. R., STOLARIK, J. D., and HEPPNER, J. P.: 1962, 'Vanguard 3 magnetic field observations', *J. Geophys. Res.* **67,** 5055–5069.

CHAPMAN, S. and BARTELS, J.: 1940, in Section 1.

DAVIS, L. R. and WILLIAMSON, J. M.: 1962, in Section 5.

DESSLER, A. J., HANSON, W. B., and PARKER, E. N.: 1961, 'Formation of the geomagnetic storm main-phase ring current', *J. Geophys. Res.* **66,** 3631–3637.

KERN, J. W.: 1962, 'A note on the generation of the main-phase ring current of a geomagnetic storm', *J. Geophys. Res.* **67,** 3737–3751.

PARKER, E. N.: 1962, 'Dynamics of the geomagnetic storm', *Space Sci. Rev.* **1,** 62–99.

SMITH, E. D. and SONETT, C. P.: 1961, 'Satellite observations of the distant field during magnetic storms: Explorer VI', *J. Phys. Soc. Japan, Intl. Conf. Cosmic Rays and Earth Storm,* Part. **1,** 17–24.